

Photon diffusion model for TTF-2

A. Jöstingmeier*, M. Dohlus* and C. Cramer†

*Deutsches Elektronen-Synchrotron DESY
Gruppe Beschleunigerphysik
Notkestr. 85, D-22603 Hamburg, Germany

†Wilhelms-Universität Münster
Institut für Physikalische Chemie
Schloßplatz 4/7, D-48149 Münster, Germany

Abstract

In this contribution it will be shown that the propagation of high-frequency electromagnetic fields in an accelerator structure may be described by a diffusion model. The parameters describing the diffusion process, i.e. diffusion constant, damping time and photon generation rate, will be determined for cavity, beam pipe and absorber sections. Then a matrix formulation will be presented which allows to calculate the steady state energy distribution in an accelerator which consists of an arbitrary sequence of these sections. The validity of the method will be checked for a variety of example structures. In order to reduce the cryogenic load of TESLA a special HOM absorber which consists of a MACOR ring was designed. The performance of such an absorber in TTF-2 will be analyzed using the developed method. The temperature rise in the absorber due to HOM losses will be calculated. The simulations require the complex permittivity spectrum in the frequency range from some GHz up to the THz regime of the absorber material as input data. We present far infrared ϵ' - and ϵ'' - spectra of MACOR at 295 K and 88 K obtained by Fourier-transform spectroscopy.

Contents

I	Introduction	2
II	Theory	3
IIa)	Lossy diffusion equation	4
IIb)	Damping times, diffusion constants and photon generation rates	6
IIb.1)	Cavity	6
IIb.2)	Beam pipe	8
IIb.3)	Absorber	11
IIc)	Matrix formulation	14
IId)	Beam excitation	18
III	Numerical results	20
IIIa)	Validation of the developed method	20
IIIb)	Absorber performance at TTF-2	24
IV	Conclusions	31

I Introduction

In [1] many aspects of the design of a HOM broadband absorber for TESLA were discussed. It was finally proposed to use a MACOR pipe in a shielding cavity in order to extract the high-frequency wakefields from the accelerating structure. The performance of such a design was investigated theoretically using a modal expansion method. For the sake of simplicity this method was applied to a staircase approximation of a TESLA 9cell cavity which is coupled to the absorber cell.

Fig.1 shows the resonant frequencies as a function of the mode number. In the frequency

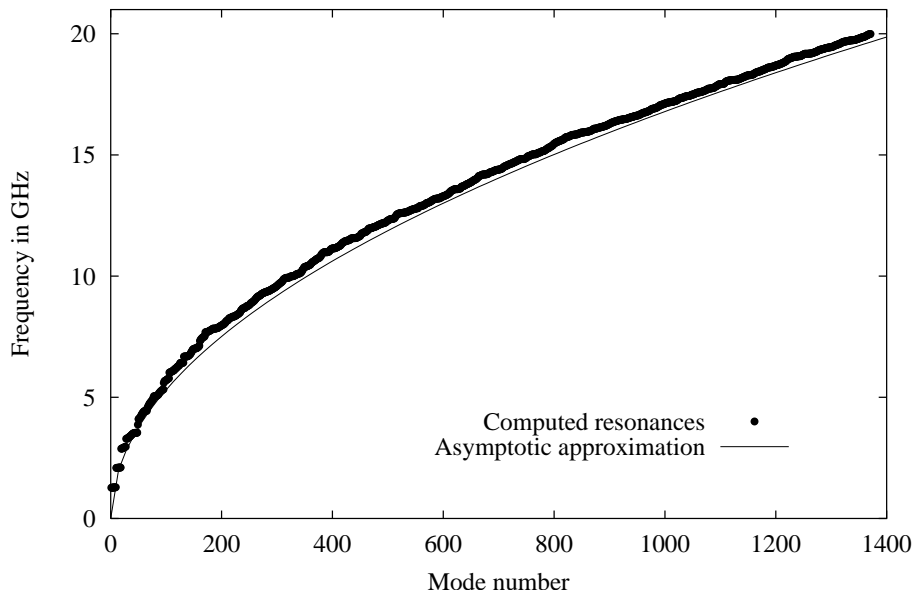


Figure 1: Resonant frequencies as a function of mode number for a TESLA 9cell cavity.

range up to 20 GHz about 1400 resonant TM monopole modes exist; and it took about one month of cpu-time on the solar cluster at DESY to calculate all these resonances. Since the mode density is proportional to the frequency it seems not to be reasonable to try to cover an even broader spectral range using a modal expansion method. Therefore another approach is required which allows us to simulate the really high-frequency wakefields in an accelerator structure within a bearable amount of cpu-time.

Recently it was suggested to use geometrical optics in order to calculate the propagation of such wakefields in a TESLA cavity. Fig.2 shows a typical path of a photon which was obtained by means of geometrical optics. The propagation of an individual photon strongly depends on its initial conditions. It will however be shown later that the propagation of many photons with randomly distributed initial conditions can be described as a diffusion process of a “photon gas”. This model will be discussed in detail in paragraph II. There it will also be demonstrated how beam pipe and absorber sections can be incorporated into the diffusion model so that a real accelerator can be analyzed.

In order to check that the MACOR ring absorber which was suggested in [1] works properly it is planned to install such an absorber in TTF-2. The developed theory will be applied to calculate the temperature rise of the absorber material as a function of the bunch length.

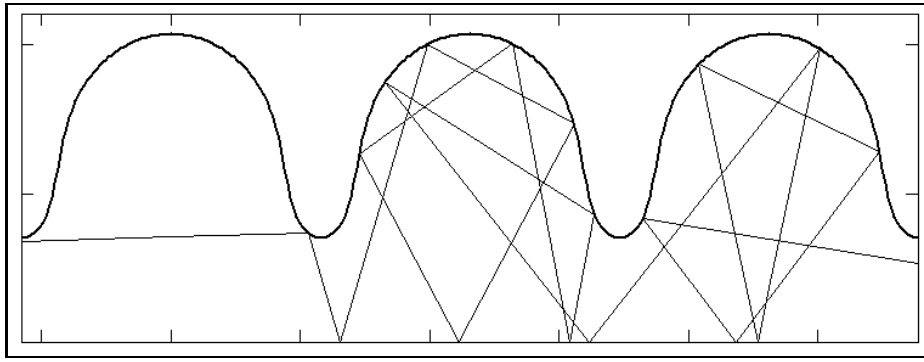


Figure 2: Propagation of a photon in a TESLA cavity.

For the simulations it is necessary to know the electromagnetic properties of the absorber material at its operational temperature in a broad frequency range. For the time being it is foreseen to use the absorber at room temperature in TTF-2; whereas it will be operated at about 70 K in TESLA. For both temperature levels we will present spectra of the complex permittivity in the far infrared region which we measured at the Universität Münster with a Fourier spectrometer. Combining the measurement results with numbers from the literature for the low and intermediate frequency range, we will obtain an accurate description of the electrical properties of MACOR at room temperature. Unfortunately corresponding numbers for an absorber temperature of 70 K and $f < 300$ GHz are still unknown. In this parameter range we hence will use an extrapolation of the available material data.

II Theory

In paragraph IIa) it will be demonstrated that the propagation of photons in a TESLA cavity is a diffusion process. A differential equation describing this process, namely the so-called lossy diffusion equation, will be derived including losses and generation of photons. The corresponding diffusion constant and the average free path length will be determined from computer simulations.

In addition to the diffusion constant we also need the damping time and the photon generation rate for a complete description of the diffusion process. These parameters will be determined in paragraph IIb) for cavity, beampipe and absorber sections. For the calculation of damping times in beampipe and absorber sections we have to determine the angular density distribution of the photons. A model of TM polarized plane waves will be used in order to compute the reflectivity of the wall material. Furthermore it will be shown that the results of the diffusion model do not depend on the exact value of the diffusion constant in beampipe and absorber sections; and it will be explained how we can get a suitable value for this quantity in such accelerator section.

In order to calculate the steady state photon density in an accelerator structure, which may consist of cavity, beampipe and absorber sections, we have to solve the lossy diffusion equation under the corresponding boundary conditions. In paragraph IIc) it will be shown how this can be done by a matrix formulation which is based on an analytic solution of the diffusion equation for each individual section (with the parameters of the diffusion model according to paragraph IIb).

For the computation of the power which is really dissipated in the HOM absorber it is

necessary to have a model for the beam excitation. Actually we need the beam impedance of the accelerating structure as a function of frequency. In paragraph II d) we make use of the result that was presented in [2]. In this contribution an analytical approximation of the δ -wake corresponding to the TESLA accelerating structure is given from which we will compute the beam impedance by a Fourier transformation.

IIa) Lossy diffusion equation

In this paragraph it will be demonstrated that the propagation of photons in a cavity is a diffusion process. Fig.3 shows the propagation of photons with different initial conditions in a

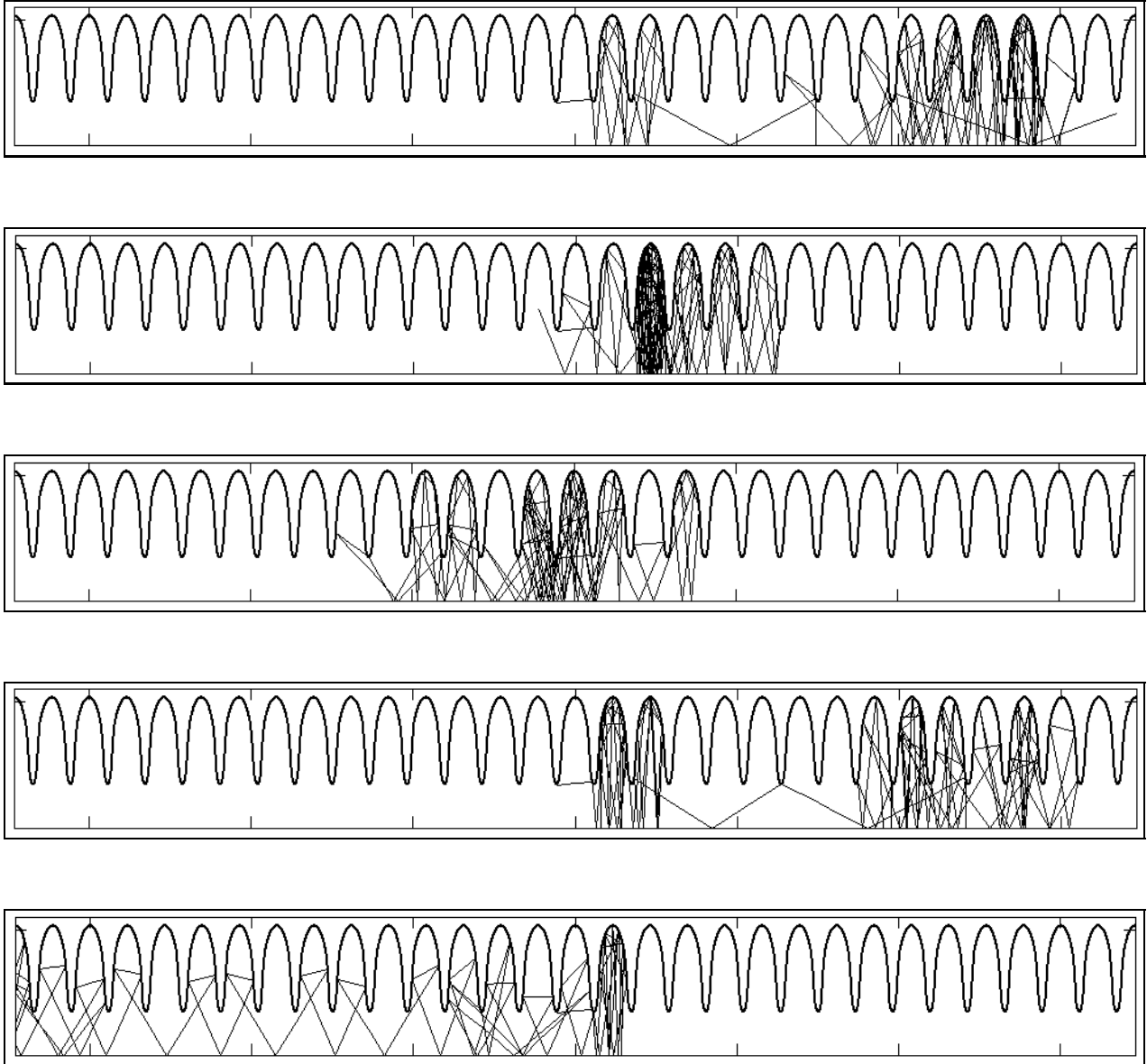


Figure 3: Propagation of photons with different initial conditions in a TESLA cavity.

TESLA cavity. The paths of the photons are calculated using geometrical optics. Fig.3 illustrates that the photons typically stay for quite a long time (for many reflections) in a confined

region of the cavity, namely within two to four consecutive cells, and then proceed several cells before they are caught again.

A more meaningful idea of the propagation process gives the histogram which is presented in Fig. 4. It shows the distribution of 1800 photons after a path length of 20 m. The photons start

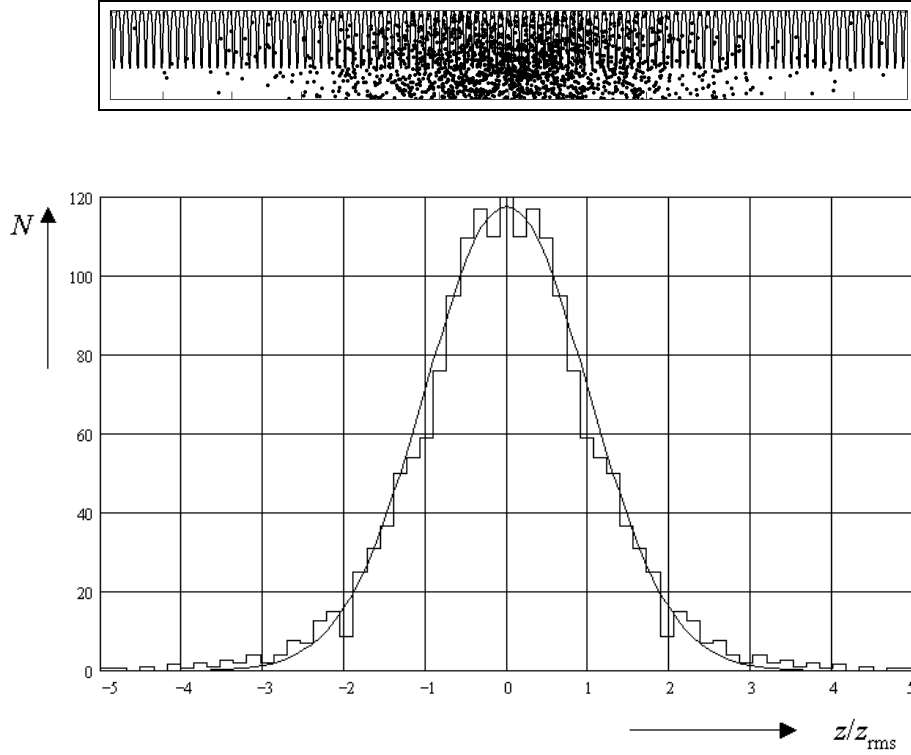


Figure 4: Distribution of 1800 photons after a path length of 20 m.

at $z = 0$ with random initial conditions. Matching the histogram with a Gaussian distribution

$$g(z) = \frac{1}{\sqrt{2\pi} z_{rms}} e^{-\frac{1}{2} \left(\frac{z}{z_{rms}}\right)^2} , \quad (1)$$

yields $z_{rms} = 1.33$ m.

Let us compare Eq. (1) with the Green's function of a one-dimensional diffusion process which is

$$\Psi_g = \frac{1}{\sqrt{4\pi Dt}} e^{-\frac{z^2}{4Dt}} , \quad (2)$$

where D is the so-called diffusion constant. Eqs. (1) and (4) are equivalent if

$$D = \frac{z_{rms}^2(t)}{2t} = \text{constant} . \quad (3)$$

If we evaluate the above equation with $z_{rms} = 1.33$ m and $t = 20 \text{ m}/c_0 = 67$ ns, where c_0 denotes the intrinsic velocity of light, we arrive at $D = 1.33 \cdot 10^7 \text{ m}^2/\text{s}$. We have also checked that D does not depend on the time t by investigating the photon distribution at other path lengths.

Since the propagation of photons in a TESLA cavity may be described by Eq. (2) we may assume that the photon density obeys the one-dimensional diffusion equation. Without absorption and generation of photons it reads

$$\frac{\partial}{\partial t} \Psi = D \frac{\partial^2}{\partial z^2} \Psi , \quad (4)$$

where Ψ denotes the photon density.

Absorption and generation of photons may be taken into account by adding two terms to the above equation:

$$\frac{\partial}{\partial t}\Psi = D \frac{\partial^2}{\partial z^2}\Psi - \frac{\Psi}{\tau} + g \quad , \quad (5)$$

where g and τ are the photon generation rate and the damping time, respectively. Eq. (5) is called “lossy diffusion equation” due to the term Ψ/τ .

Another important parameter which we need for our further analysis is the average free path length z_f which is defined as

$$z_f = \text{average over all photons} \left(\frac{c_0 t}{\text{number of reflections}} \right) \quad . \quad (6)$$

The simulations show that z_f is about 150 mm which is roughly twice the diameter of the iris.

IIb) Damping times, diffusion constants and photon generation rates

IIb.1) Cavity

The diffusion constant of a TESLA cavity was already determined in paragraph IIa). For this type of structure it still remains to calculate the damping time and the photon generation rate.

Let us start with the cavity damping time τ which is defined as

$$\frac{1}{\tau} = \frac{-\frac{dW}{dt}}{W} \quad , \quad (7)$$

where W is the total stored energy. The relative energy loss rate, which is just the R.H.S. of Eq. (7), is obviously given by the relative energy loss at a single reflection $1 - |r|^2$ divided by the average time of flight of a photon between two reflections. Thus we have

$$\frac{1}{\tau} = \frac{1 - |r|^2}{t_f} \quad . \quad (8)$$

Keeping in mind that t_f is related to the average free path length of a photon by

$$t_f = \frac{z_f}{c_0} \quad , \quad (9)$$

we arrive at

$$\tau = \frac{z_f}{c_0 (1 - |r|^2)} \quad (10)$$

for the damping time of a cavity.

In order to determine $|r|^2$ let us assume that the electromagnetic field can locally be approximated by a TEM wave. The reflection coefficient is in general a function of frequency and a function of the angle of incidence of the incoming field onto the cavity surface. It can be however shown that the reflection at a metal surface is almost independent of this angle [3]:

$$|r|^2 \approx \left| \frac{Z_{met} - Z_0}{Z_{met} + Z_0} \right|^2 \quad \text{with} \quad Z_{met} \approx \sqrt{\frac{j\omega\mu_0}{\sigma}} = (1 + j) \underbrace{\sqrt{\frac{\omega\mu_0}{2\sigma}}}_{R_s} \quad , \quad (11)$$

where R_s denotes the real part of the surface impedance of the cavity wall material. Eliminating Z_{met} from Eq. (11), finally yields

$$1 - |r|^2 \approx 4 \frac{R_s}{Z_0} . \quad (12)$$

This leads to the following approximation for the cavity damping time:

$$\tau \approx \frac{Z_0}{4R_s} \frac{z_f}{c_0} \quad (13)$$

Fig. 5 presents the real part of the surface impedance of niobium at 2 K as a function of

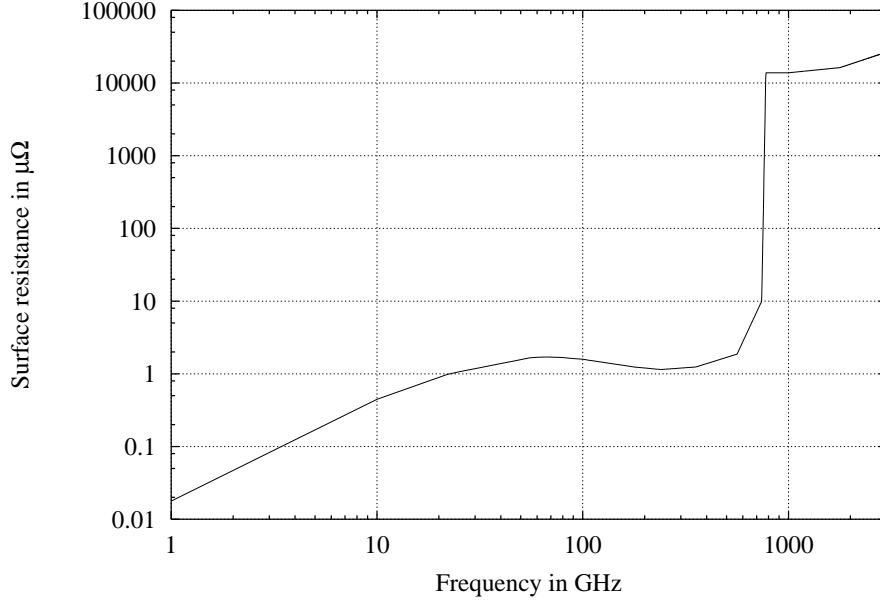


Figure 5: Real part of the surface resistance of niobium at 2 K as a function of frequency.

frequency. Note that the surface resistance increases by approximately four orders of magnitude between 600 GHz and 800 GHz where the photon energy becomes large enough to crack the Cooper pairs.

Fig. 6 shows the corresponding damping time of a TESLA cavity as a function of frequency. For the calculation of τ we assume an average free path length of the photons of 150 mm. This number was already given in paragraph IIa). From the curve shown in Fig. 6 we can conclude that the cavity damping time is about 30 ms between 20 GHz and 600 GHz. For higher frequencies τ drops dramatically according to the behaviour of the surface resistance in this frequency range.

The generation of wakefields takes basically place in the cavities of a linear accelerator. For the sake of simplicity let us assume that we can neglect the photon generation in the beampipe and absorber sections of the investigated structures. It is obvious that the photon generation rate $g(z, t)$ is proportional to the beam current I_b . If we furthermore assume that this quantity is independent of time and the axial coordinate in a cavity, we can write for $g(z, t)$

$$g(z, t) \propto I_b \cdot \begin{cases} 1 & , \text{ if } z \text{ in cavity} \\ 0 & , \text{ otherwise} \end{cases} . \quad (14)$$

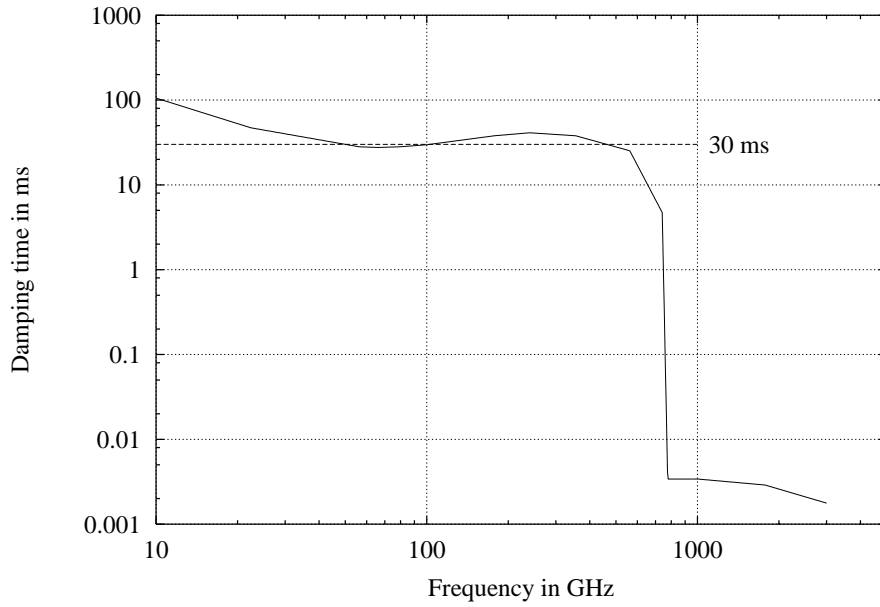


Figure 6: Damping time of a TESLA cavity as a function of frequency.

I Ib.2) Beampipe

The average free path length in a beampipe is given by

$$z_f = \frac{2a}{\sin\alpha} \quad (15)$$

according to Fig. 7. The quantities a and α denote the radius of the beampipe and the angle

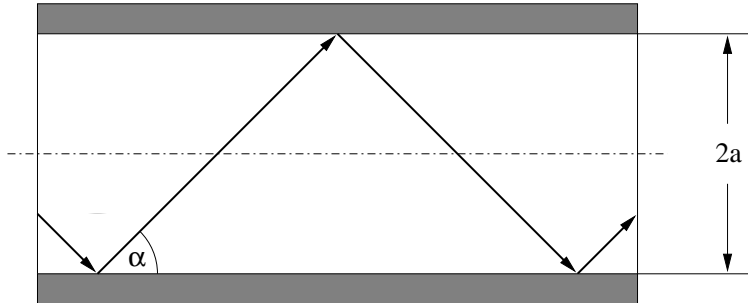


Figure 7: Path of a photon in a circular waveguide.

between the beampipe axis and the direction of propagation of the photon.

The calculation of the beampipe damping time is slightly different from the determination of this quantity for a cavity. As a photon propagates through a cavity it is reflected back and forth and can in principle move in any direction during this process. On the other hand, Fig. 7 illustrates that in a beampipe a photon basically keeps its direction of motion - only the sign of the angle α flips after each reflection. For the computation of an effective beampipe damping time we thus have to take the angular density distribution of the photons into account and the

fact that the reflection coefficient of a photon at the beampipe wall is not only a function of frequency but also a function of the angle of propagation.

Fig.8 shows the model that we use for the calculation of the angular distribution of the

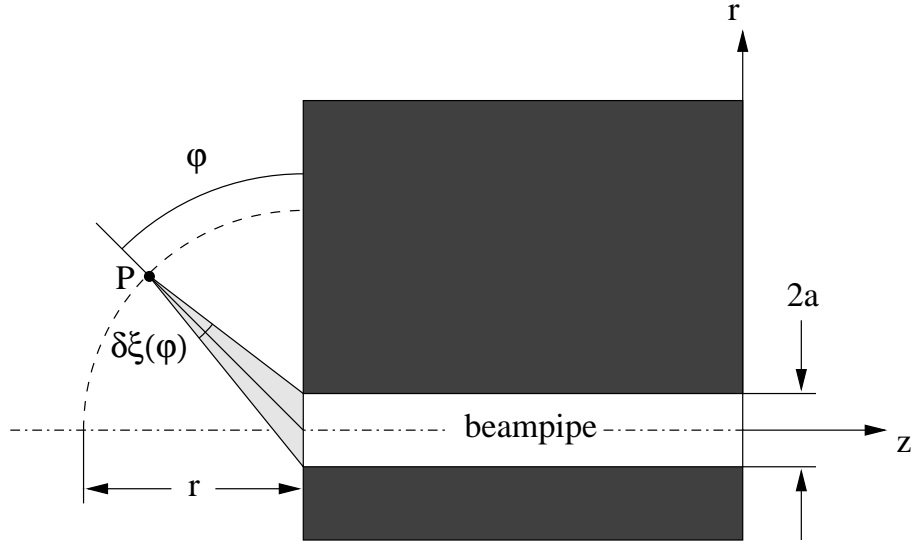


Figure 8: Angular distribution of photons in a beampipe.

photons. Due to their chaotic movement in a cavity we can assume that their angular density distribution in such a kind of structure is almost independent of φ . Note that for the further analysis it is more convenient to use the angle φ instead of α which was defined in Fig. 7. These two angles are related by

$$\varphi = \alpha + \frac{\pi}{2} \quad \text{with} \quad -\frac{\pi}{2} \leq \alpha \leq +\frac{\pi}{2} \quad . \quad (16)$$

If we assume that the point P from which the photons emerge is far away from the beampipe ($r \gg 2a$) it follows from elementary geometric considerations that

$$\delta\xi(\varphi) \propto \sin\varphi \quad . \quad (17)$$

The above relation means that the beampipe aperture has a maximum for photons which propagate along the z -axis of the beampipe, namely for $\varphi = \pi/2$. On the other hand, there are no photons in the beampipe which move perpendicular to the z -axis ($\varphi = 0$ or $\varphi = \pi$). Normalizing $\delta\xi(\varphi)$ yields

$$\frac{\delta\xi(\varphi)}{\langle \delta\xi(\varphi) \rangle_\varphi} = \frac{\sin\varphi}{2} \quad (18)$$

with

$$\langle \dots \rangle_\varphi = \int_{\varphi=0}^{\pi} \dots d\varphi \quad . \quad (19)$$

For the calculation of the reflection coefficient of a photon at a beampipe wall we use the model of a TM polarized plane wave which is reflected at the plane surface of a good conductor. For such a configuration it can be shown that

$$|r(\omega, \varphi)| \approx \left| \frac{|\cos\varphi| - \frac{Z_{met}}{Z_0}}{|\cos\varphi| + \frac{Z_{met}}{Z_0}} \right| \quad , \quad (20)$$

with Z_{met} according to Eq. (11). In order to compute the damping time of a beampipe we can again apply Eq. (10) which was originally derived for a cavity. Note that for a beampipe section the expressions which have to be inserted for z_f and r are given by Eqs. (15) and (20). This means that the damping time of a beampipe is also a function of φ which is not the case for that of a cavity.

An effective damping time of a beampipe $\bar{\tau}(\omega)$ may be defined by averaging $\tau(\omega, \varphi)$ over φ :

$$\frac{1}{\bar{\tau}(\omega)} = \left\langle \frac{\delta\xi(\varphi)}{\langle\delta\xi(\varphi)\rangle_\varphi} \frac{1}{\tau(\omega, \varphi)} \right\rangle_\varphi \quad (21)$$

In the above equation the non-uniform angular density distribution of the photons is taken into account by the term $\delta\xi(\varphi)/\langle\delta\xi(\varphi)\rangle_\varphi$ which is given by Eq. (18).

The damping times as a function of frequency of a steel and a copper beampipe with a radius of 35 mm are shown in Fig. 9. For steel and copper we assume conductivities of $\sigma = 0.5 \cdot 10^7$ S/m and $\sigma = 5.8 \cdot 10^7$ S/m, respectively. As expected, the damping time of a steel pipe is significantly less than that of a corresponding copper pipe. Keeping in mind that the corresponding quantity of a TESLA cavity is about 30 ms in the frequency range between 20 GHz and 600 GHz, see Fig. 6, it is interesting to note that the damping times of the considered beampipes are well below $1 \mu\text{s}$ in this frequency range.

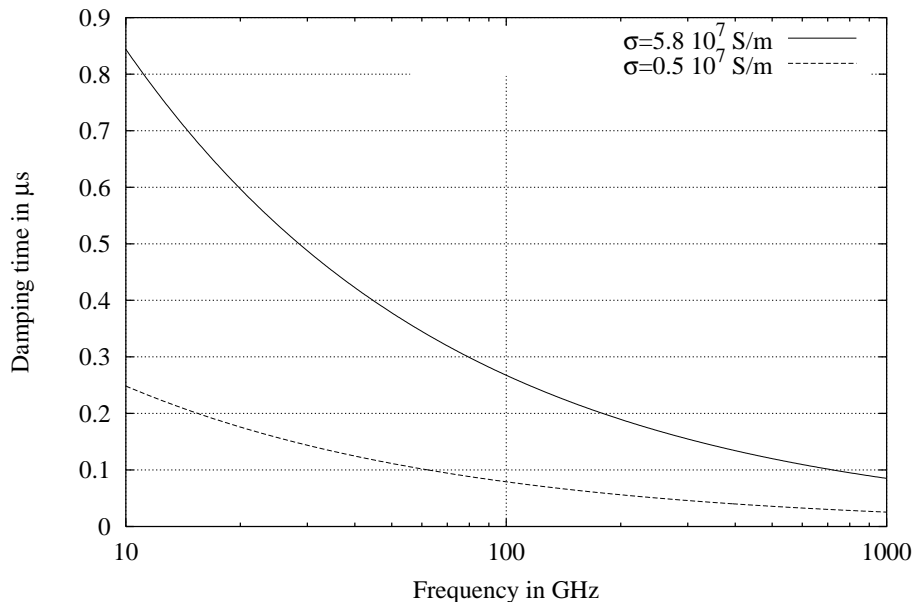


Figure 9: Damping time of a beampipe with a radius of 35 mm as a function of frequency for a wall conductivity of $\sigma = 5.8 \cdot 10^7$ S/m and $\sigma = 0.5 \cdot 10^7$ S/m.

The propagation of photons in a beampipe is actually not a diffusion process. Nevertheless we can also use our diffusion model for the such sections for the following reason: Photons traverse a beampipe much faster than a cavity of the same length. This means that significant variations of the energy density cannot build up. Consequently the simulation results of the diffusion model do not really depend on the exact value of the diffusion constant of such a section. It is sufficient to assume a value for this quantity which is large compared with that of a cavity.

Let us illustrate this assumption for a monofrequent electromagnetic wave in a beampipe with small losses. The energy density in the longitudinal direction w in such a waveguide can be written as

$$w = w_0 e^{-2\alpha z} \quad , \quad (22)$$

where w_0 denotes w at the axial coordinate $z = 0$; and α is the corresponding attenuation coefficient. The gradient of the energy density reads

$$\frac{dw}{dz} = -2\alpha w \quad . \quad (23)$$

Keeping in mind that the energy density and the power of a waveguide mode are related by the group velocity v_g

$$w = \frac{p}{v_g} \quad , \quad (24)$$

yields

$$p = - \underbrace{\frac{v_g}{2\alpha}}_D \frac{dw}{dz} \quad . \quad (25)$$

The above equation corresponds to a diffusion process of the photons along the gradient of the energy density which itself is equivalent to the photon density. Thus we can identify the term $v_g / (2\alpha)$ as something like a “diffusion constant”. Let us assume that the group velocity is close to c_0 and that α is 0.1 dB/m (which is a typical value for a TM_{01} wave at 300 GHz in a circular waveguide with a radius of 35 mm that is made out of copper), then we get $6 \cdot 10^{10} \text{ m}^2/\text{s}$ for D . This value is considerably higher than the diffusion constant of a TESLA cavity which is $1.33 \cdot 10^7 \text{ m}^2/\text{s}$.

IIb.3) Absorber

In our design a HOM absorber section consists of a metal-backed pipe of absorber material. The treatment of such a section is thus very similar to that of a beampipe. The only difference in the analysis of a beampipe and an absorber section is that we have to substitute the formula for the reflection coefficient according to Eq.(20) by a corresponding one for an absorber.

Let us again apply the model of a plane wave which is reflected at the vacuum-absorber interface as it is shown in Fig.10. The electromagnetic field is TM polarized. The incident and the reflected wave are marked by the superscripts “i” and “r”. The quantities k_0 and k denote the vacuum wavenumber and the corresponding quantity in the absorber material. The thickness of this material is d . The incident and the reflected magnetic field are given by

$$\mathbf{H}^i = \mathbf{e}_x H_0 e^{-jk_0(\sin\varphi z - \cos\varphi y)} \quad , \quad (26)$$

$$\mathbf{H}^r = \mathbf{e}_x r H_0 e^{-jk_0(\sin\varphi z + \cos\varphi y)} \quad , \quad (27)$$

where \mathbf{e}_x and H_0 are the unit vector in the x -direction and the amplitude of the incident magnetic field. It can be shown that the reflection coefficient r which is defined by Eqs.(26) and (27) reads

$$r(\omega, \varphi) = \frac{|\cos\varphi| - \frac{k_y}{\omega\epsilon Z_0} j \tan(k_y d)}{|\cos\varphi| + \frac{k_y}{\omega\epsilon Z_0} j \tan(k_y d)} \quad , \quad (28)$$

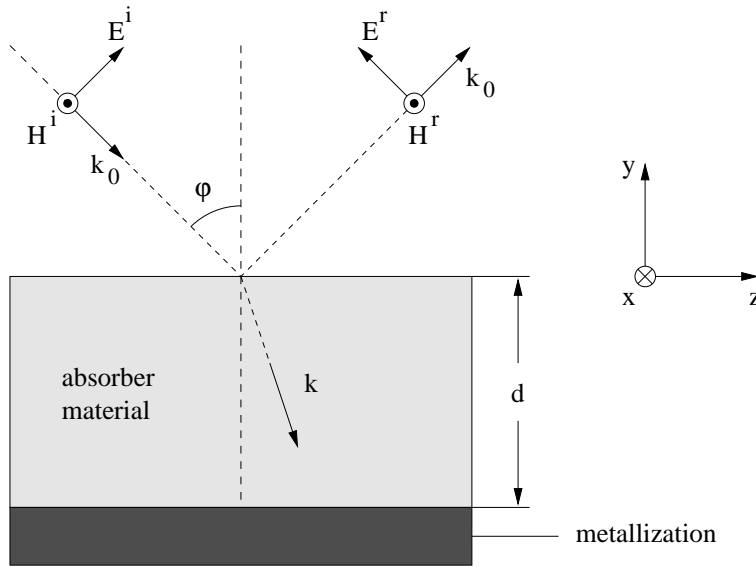


Figure 10: Reflection of a plane wave at the vacuum - absorber interface.

where k_y is the y -component of the wavenumber in the absorber material:

$$k_y = k_0 \sqrt{\varepsilon_r - \sin^2 \varphi} \quad (29)$$

The quantities ε and ε_r denote the absolute and the relative permittivity of this material, respectively. Summarizing this paragraph we can say that the damping time of an absorber can be calculated in the same way as that of a beampipe. We have simply to use Eq. (28) for the reflection coefficient instead of Eq. (20).

For the computation of the damping time of a MACOR absorber we need the complex permittivity of this material. Since very short bunches are foreseen for the FEL operation mode of TESLA it is necessary to know the electrical properties of MACOR in a broad spectral range.

We measured the complex permittivity of MACOR in the frequency range from 300 GHz to about 1.5 THz using a Fourier transform infrared spectrometer (FTIR-spectrometer: BOMEM DA 8.1). The measurements were carried out at room temperature and at 88 K which was the lowest temperature that we could reach with the available cooling system. A brief description of the measurement principle can be found in the Appendix. It turned out that the real part of the permittivity is almost frequency and temperature independent and lies between 5.6 and 5.7. However this does not hold for the losses. The measured imaginary part of ε_r is shown in Fig. 11.

If we combine the measurement results at room temperature with numbers from the literature we obtain a loss spectrum of MACOR ranging from 8.5 GHz to 1.6 THz. Unfortunately there is no data available for this material at the low temperature level for frequencies less than 300 GHz. In this parameter range we scale the corresponding room temperature values by using the ratio of the losses at 88 K and 295 K at a frequency of 300 GHz as a scaling factor. Both spectra are shown in Fig. 12.

Fig. 13 presents the damping time of a MACOR absorber ring at room temperature as a function of frequency with the thickness of the ring as a parameter. The damping times of the 10 mm and the 30 mm absorber are almost identical for high frequencies ($f > 200$ GHz). In this

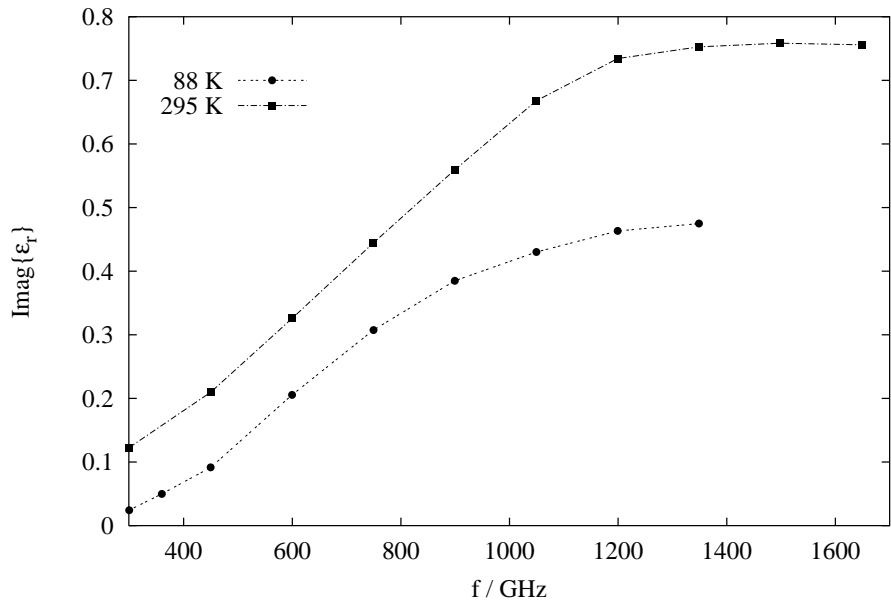


Figure 11: Imaginary part of the permittivity of MACOR at 295 K and 88 K as a function of frequency in the far infrared range.

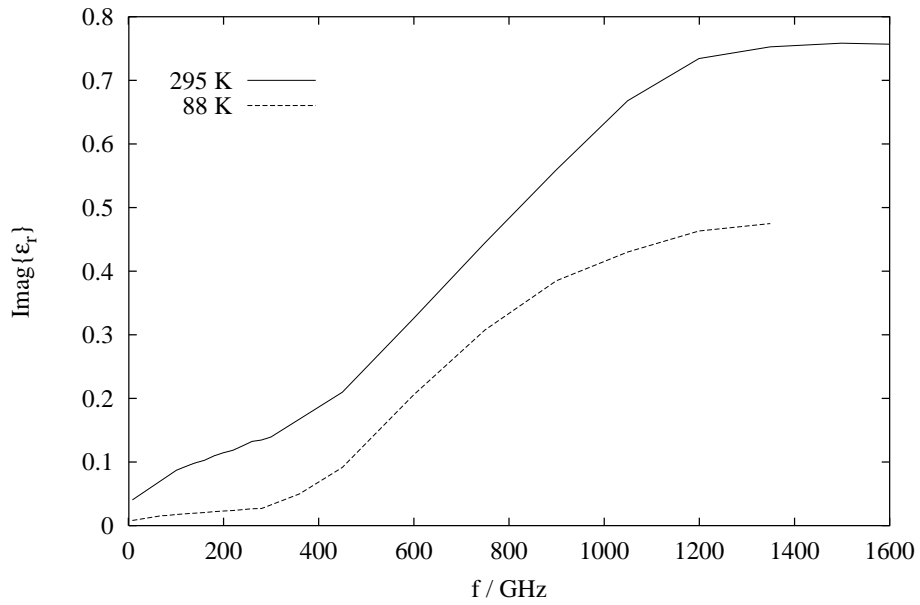


Figure 12: Imaginary part of the permittivity of MACOR at room temperature and at 88 K in the range from 8.5 GHz to $f > 1$ THz.

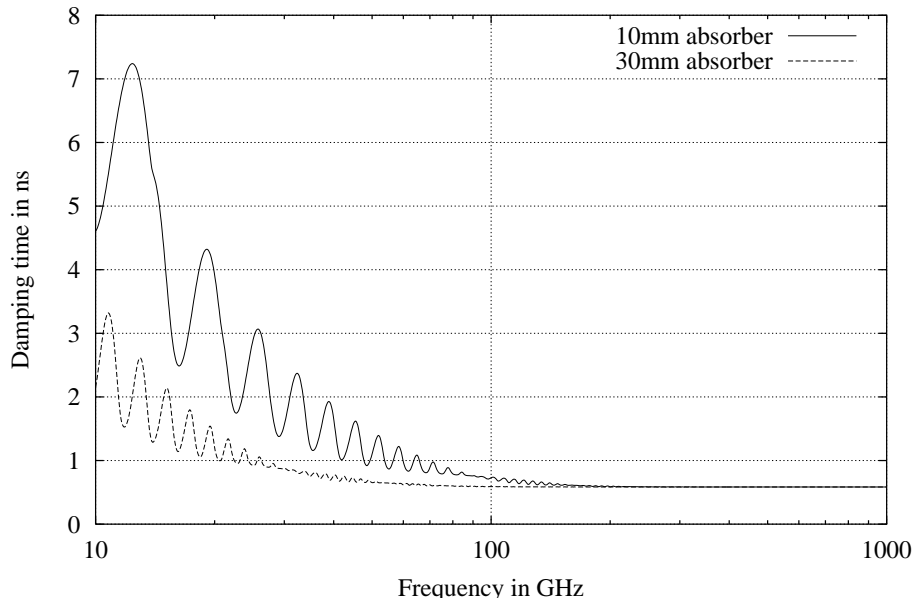


Figure 13: Damping time of a MACOR absorber ring at room temperature as a function of frequency with the thickness of the ring as a parameter.

frequency range the absorption of MACOR becomes so strong that an incoming electromagnetic wave does not “see” the metallization behind the absorber material. Consequently, the reflection coefficient at the absorber surface does not depend on the thickness of the MACOR ring in this case.

On the other hand, Fig. 13 also illustrates that the damping time of the absorber can significantly be reduced for low frequencies if we increase the thickness of the ring. The curves show relatively strong oscillations in the low frequency range due to interference. As expected, the spectral distance between two maxima of the 30 mm absorber is one third of that corresponding to the 10 mm absorber.

Fig. 14 shows the corresponding damping times for an absorber at 88 K. If we compare the curves which are presented in Figs. 13 and 14 we see that in the 88 K case the damping times are much higher than those of MACOR at room temperature. This indicates that the absorber efficiency is reduced if we use it at a lower temperature level. However, for very high frequencies ($f > 400$ GHz) we have the same value for the damping time as for the absorber at room temperature. This demonstrates that the high-frequency performance of an absorber material only depends on the real part of its permittivity.

IIc) Matrix formulation

In this paragraph we will develop a matrix formulation which allows us to compute the steady state energy density in a structure that consists of consecutive cavity, beampipe and absorber sections. The time-dependent lossy diffusion equation which was discussed in paragraph IIa) reads

$$\frac{\partial \Psi}{\partial t} + \frac{\partial \Phi}{\partial z} = -\frac{\Psi}{\tau} + g \quad . \quad (30)$$

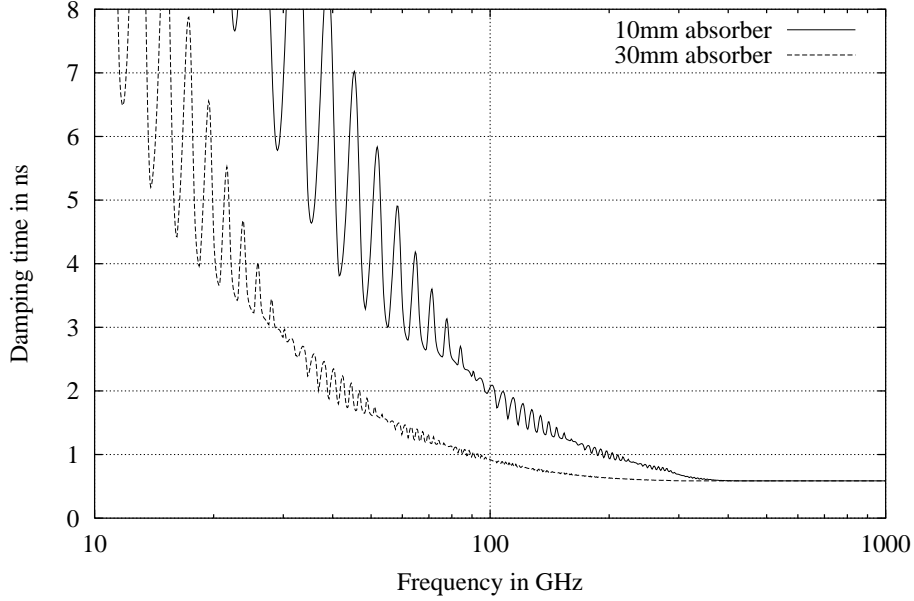


Figure 14: Damping time of a MACOR absorber ring at 88 K as a function of frequency with the thickness of the ring as a parameter.

In paragraph IIa) Ψ and Φ were defined as the photon density and the photon flux density. For a fixed frequency Ψ and Φ are proportional to the energy density and the power density in the positive z -direction, respectively. Since these quantities are more convenient for our analysis than numbers of photons we redefine Ψ and Φ correspondingly.

In the steady state the quantities Ψ , Φ and g are time-independent and will be marked by the index 0. Keeping in mind that the power density Ψ_0 is related to the energy density Φ_0 by

$$\Phi_0 = -D \frac{\partial \Psi_0}{\partial z} \quad (31)$$

and inserting the above equation into Eq. (30) yields the differential equation

$$\frac{\partial \Psi_0^2(z)}{\partial z^2} - \frac{1}{D} \frac{\Psi_0(z)}{\tau} = -\frac{g_0}{D} \quad (32)$$

which governs the steady state of the lossy diffusion process.

For each individual section of a composed accelerator structure the damping time, the diffusion constant and the photon generation rate do not depend on the axial coordinate z . Hence the energy density and the power density in each section can be calculated straightforwardly as a function of the corresponding initial values $\Psi_0(0)$ and $\Phi_0(0)$ at the beginning of the section:

For the sake of simplicity, let us introduce two new quantities

$$L_d = \sqrt{D\tau} \quad , \quad (33)$$

$$v_d = \sqrt{\frac{D}{\tau}} \quad (34)$$

which are the diffusion length and the diffusion velocity, respectively. The general solution of Eq. (32) reads

$$\Psi_0(z) = \tau g_0 + A e^{-\frac{z}{L_d}} + B e^{+\frac{z}{L_d}} \quad , \quad (35)$$

$$\Phi_0(z) = v_d \left(A e^{-\frac{z}{L_d}} - B e^{+\frac{z}{L_d}} \right) \quad (36)$$

where A and B are integration constants which still have to be determined from the initial conditions. The values of $\Psi_0(z)$ and $\Phi_0(z)$ at $z = 0$ are abbreviated by

$$\Psi_0(0) = \Psi_{01} \quad , \quad (37)$$

$$\Phi_0(0) = \Phi_{01} \quad . \quad (38)$$

Using the above definitions, the integration constants are

$$A = \frac{1}{2} \left(-\tau g_0 + \Psi_{01} + \frac{\Phi_{01}}{v_d} \right) \quad , \quad (39)$$

$$B = \frac{1}{2} \left(-\tau g_0 + \Psi_{01} - \frac{\Phi_{01}}{v_d} \right) \quad . \quad (40)$$

If we insert Eqs. (39) and (40) into Eqs. (35) and (36), we obtain Ψ_0 and Φ_0 at the end of the section, at $z = L$, in terms of Ψ_{01} and Φ_{01} :

$$\Psi_0(L) = \Psi_{02} = \Psi_{01} \cosh\left(\frac{L}{L_d}\right) - \frac{\Phi_{01}}{v_d} \sinh\left(\frac{L}{L_d}\right) + \tau g_0 \left(1 - \cosh\left(\frac{L}{L_d}\right)\right) \quad , \quad (41)$$

$$\Phi_0(L) = \Phi_{02} = -\Psi_{01} v_d \sinh\left(\frac{L}{L_d}\right) + \Phi_{01} \cosh\left(\frac{L}{L_d}\right) + L_d g_0 \sinh\left(\frac{L}{L_d}\right) \quad (42)$$

Eqs. (41) and (42) can be written concisely in matrix notation:

$$\begin{pmatrix} \Psi_{02} \\ \Phi_{02} \end{pmatrix} = \begin{pmatrix} \cosh\left(\frac{L}{L_d}\right) & -\frac{1}{v_d} \sinh\left(\frac{L}{L_d}\right) \\ -v_d \sinh\left(\frac{L}{L_d}\right) & \cosh\left(\frac{L}{L_d}\right) \end{pmatrix} \begin{pmatrix} \Psi_{01} \\ \Phi_{01} \end{pmatrix} + \tau g_0 \begin{pmatrix} 1 - \cosh\left(\frac{L}{L_d}\right) \\ v_d \sinh\left(\frac{L}{L_d}\right) \end{pmatrix} \quad (43)$$

Up to this point of the analysis we only have considered one single section of a composed structure. In order to investigate a cascade of such sections we must discuss how the quantities Ψ_{02} and Φ_{02} of the n th section, Ψ_{02}^n and Φ_{02}^n , are to be translated into the initial conditions of the $(n+1)$ th structure, Ψ_{01}^{n+1} and Φ_{01}^{n+1} . Assuming that the energy density and the power flow are continuous along the structure, the following continuity relations are valid at the connection of the n th and the $(n+1)$ th section:

$$\Psi_{01}^{n+1} = \Psi_{02}^n \quad , \quad (44)$$

$$A^{n+1} \Phi_{01}^{n+1} = A^n \Phi_{02}^n \quad , \quad (45)$$

where A^{n+1} and A^n are the cross sectional areas of the corresponding sections¹. Since we are dealing with circular symmetric structures, for which the cross sectional area is proportional to the radius squared, Φ_{01}^{n+1} and Φ_{02}^n are related by

$$\Phi_{01}^{n+1} = \left(\frac{r^n}{r^{n+1}} \right)^2 \Phi_{02}^n \quad , \quad (46)$$

¹Note that Eq. (45) is not as trivial as it might appear at first sight. It is based on the assumption that the power density is uniform over the cross section of the structure. This implies that the same statement is also true for the energy density. On the other hand it is well-known that this quantity is proportional to the inverse of the radius for TM_0 modes in perfectly circular symmetric structures. Eq. (45) consequently does not hold for this case. For real structures we may however assume that this equation is valid, at least for high frequencies ($f > 300$ GHz) where small imperfections, such as surface roughness of the wall material or small distortions of the symmetry, lead to a uniform distribution of the energy over the cross section of the structure.

where r^n and r^{n+1} are the radii of the n th and the $(n + 1)$ th section. Eqs. (44) and (46) read in matrix notation

$$\begin{pmatrix} \Psi_{01}^{n+1} \\ \Phi_{01}^{n+1} \end{pmatrix} = \begin{pmatrix} 1 & 0 \\ 0 & \left(\frac{r^n}{r^{n+1}}\right)^2 \end{pmatrix} \begin{pmatrix} \Psi_{02}^n \\ \Phi_{02}^n \end{pmatrix} . \quad (47)$$

Eq. (43) tells us how the energy density and the power density at the end of a section, Ψ_{02} and Φ_{02} , respectively, are related with the corresponding quantities Ψ_{01} and Φ_{01} at the beginning of this section. Moreover, the continuity conditions between the energy density and the power density at the end of a section and the corresponding initial conditions at the beginning of the next section are given by Eq. (47). We can thus calculate the linear relations between Ψ and Φ at the beginning and at the end of the entire structure by simply multiplying the matrices which characterize the individual sections and their interconnections:

$$\begin{pmatrix} \Psi_{02}^N \\ \Phi_{02}^N \end{pmatrix} = \begin{pmatrix} m_{11} & m_{12} \\ m_{21} & m_{22} \end{pmatrix} \begin{pmatrix} \Psi_{01}^1 \\ \Phi_{01}^1 \end{pmatrix} + \begin{pmatrix} c_1 \\ c_2 \end{pmatrix} \quad (48)$$

If we assume that the power densities Φ_{01}^1 and Φ_{02}^N vanish

$$\Phi_{02}^N = 0 = m_{21}\Psi_{01}^1 + m_{22}\underbrace{\Phi_{01}^1}_{=0} + c_2 , \quad (49)$$

then the energy density at the beginning of the structure reads

$$\Psi_{01}^1 = -\frac{c_2}{m_{21}} . \quad (50)$$

Knowing Ψ_{01}^1 and Φ_{01}^1 , we can compute all quantities Ψ_{01}^n and Φ_{01}^n using Eqs. (43) and (47). The integration constants A and B of each individual section are then given by Eqs. (39) and (40). If we insert these constants into Eqs. (35) and (36) we obtain the energy density and the power density as a function of the axial coordinate z in each section.

In order to measure the performance of an absorber we have to calculate the power loss and generation in the individual sections. Let the superscript n denote the number of a section. The generated HOM power P_{wake}^n in the n th section is just

$$P_{wake}^n = \pi (r^n)^2 g_0^n L^n . \quad (51)$$

The power loss in the n th section is on the other hand determined by the difference of the powers at the entrance and the exit of this section, $\pi (r^n)^2 \Phi_{01}^n$ and $\pi (r^n)^2 \Phi_{02}^n$, respectively, and the power $\pi (r^n)^2 g_0^n L^n$ generated in this section:

$$P_{loss}^n = \pi (r^n)^2 (-\Phi_{02}^n + \Phi_{01}^n + g_0^n L^n) \quad (52)$$

The above equation can be reformulated:

$$P_{loss}^n = \pi (r^n)^2 \left(-\int_{z=z_1^n}^{z_2^n} \frac{d\Phi_0}{dz} dz + g_0^n L^n \right) \quad (53)$$

Inserting Eq. (30) with $\frac{\partial \Psi}{\partial t} = 0$ into Eq. (53), yields

$$P_{loss}^n = \frac{\pi (r^n)^2}{\tau^n} \int_{z=z_1^n}^{z_2^n} \Psi_0 dz \quad . \quad (54)$$

Note that Eq. (54) no longer contains the term $\pi (r^n)^2 g_0^n L^n$ which describes the photon generation. The above equation can be evaluated with $\Psi_0(z)$ according to Eq. (35):

$$P_{loss}^n = \pi (r^n)^2 \left(g_0^n L^n - A^n v_d^n \left(e^{-\frac{L^n}{L_d^n}} - 1 \right) + B^n v_d^n \left(e^{+\frac{L^n}{L_d^n}} - 1 \right) \right) \quad (55)$$

The total wakefield power which is generated in the entire structure is the sum of the contributions corresponding to the individual sections:

$$P_{wake}^{tot} = \sum_{n=1}^N P_{wake}^n \quad (56)$$

For the further analysis it is convenient to establish a relation between the total generated wakefield power and the power loss in the HOM absorber:

$$\eta(\omega) = \frac{P_{loss}^{abs}}{P_{wake}^{tot}} \quad (57)$$

P_{loss}^{abs} denotes the power loss in the HOM absorber which is that one of the P_{loss}^n which corresponds to the absorber section; and the quantity $\eta(\omega)$ is something like an absorber efficiency. The higher the value of $\eta(\omega)$ is, the more of the generated wakefield power is dissipated in the HOM absorber.

IId) Beam excitation

The TESLA accelerator basically consists of a periodic array of cavities. The wakefield induced by a single cavity can be calculated with good accuracy using a diffraction model which was described in detail in [4]. The wakefield in a periodic structure is however not the sum of the individual single cavity contributions. This can be explained by the fact that the electromagnetic field which travels with the bunch is already modified by the upstream cavities.

Talking about periodic structures we have to keep in mind that TTF-2 only contains 7 accelerating modules. Thus we have to put forward the question whether the results for the periodic regime can already be applied to TTF-2. In [2] it was shown that there is still a significant difference between the wakefields for the first and the second module if one assumes a bunch length of 50 μm . The scheduled bunch length for TTF-2 lies somewhere between 50 μm and 100 μm . For the sake of simplicity let us assume however that TTF-2 can be treated as a periodic structure.

The power loss due to the self-wake of the bunches is given by the formula

$$P_{wake}^{tot} = q^2 N_b f_r k_l \quad , \quad (58)$$

where q , N_b , f_r and k_l denote the bunch charge, the number of bunches per bunch train, the repetition frequency and the loss parameter which can be calculated from the relation

$$k_l = \frac{1}{\pi} \int_{\omega=0}^{\infty} \text{Re}\{Z(\omega)\} |\tilde{\lambda}(\omega)|^2 d\omega \quad . \quad (59)$$

The term $\text{Re}\{Z(\omega)\}$ is the real part of the beam impedance; whereas $\tilde{\chi}(\omega)$ denotes the bunch spectrum. Note that P_{wake}^{tot} was already defined in Eq. (56) as the sum of all P_{wake}^n . This means that we must use the beam impedance of the entire structure for $Z(\omega)$ in the previous equation and not that of a single cavity or module.

In order to make use of Eq. (59) we must know the real part of the beam impedance of the TESLA accelerating structure. The wakefields of Gaussian bunches in this structure with σ ranging from $50 \mu\text{m}$ to $1000 \mu\text{m}$ were simulated in [2]. There it was also shown how one can obtain an analytical approximation of the δ -wake as an envelope function which is common to the wakefields of the different bunches. The analytical approximation reads

$$W_{\delta}(s) = 315 \text{ V/pC} \cdot \left(1.165 \cdot e^{-\sqrt{s/3.65 \text{ mm}}} - 0.165 \right) . \quad (60)$$

We can calculate the beam impedance $Z(\omega)$ from the above formula by a Fourier transformation. Fig. 15 shows the real part $Z(\omega)$ of a TESLA 9cell cavity as a function of frequency.

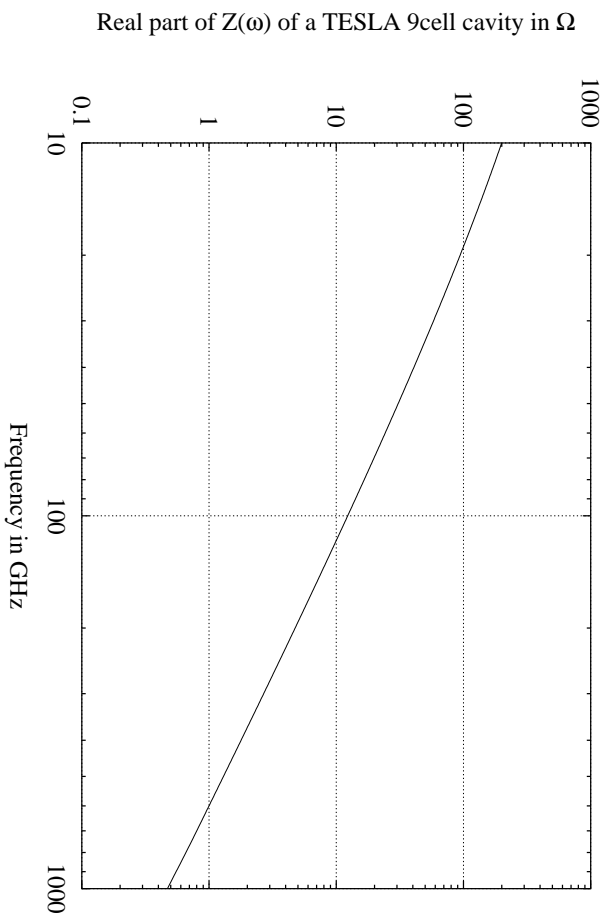


Figure 15: Real part of the beam impedance of a TESLA 9cell cavity as a function of frequency.

From Eq. (59) it follows that the power loss in the frequency interval $d\omega$ is just

$$dP_{wake}^{tot} = q^2 N_b f_r \frac{1}{\pi} \text{Re}\{Z(\omega)\} |\tilde{\chi}(\omega)|^2 d\omega . \quad (61)$$

Usually a Gaussian distribution is assumed for the bunch shape. The corresponding spectrum is

$$\tilde{\chi}(\omega) = e^{-\frac{1}{2} \left(\frac{\omega \sigma}{\omega_c} \right)^2} , \quad (62)$$

with

$$\omega_c = \frac{c_0}{\sigma} . \quad (63)$$

By making use of the absorber efficiency $\eta(\omega)$ which was defined in Eq. (57), we can calculate the power which is dissipated in the HOM absorber in the frequency interval ranging from ω_1

to ω_2 as

$$P_{loss}^{abs}(\omega_1, \omega_2) = q^2 N_b f_r \frac{1}{\pi} \int_{\omega=\omega_1}^{\omega_2} \eta(\omega) \operatorname{Re}\{Z(\omega)\} |\tilde{\lambda}(\omega)|^2 d\omega \quad . \quad (64)$$

The above integration is carried out numerically in our simulation routine.

III Numerical results

Paragraph IIIa) is dedicated to the validation of the developed method. A variety of example structures will be investigated in order to show the effect of the individual model parameters, such as diffusion constant, damping time, photon generation rate etc., on the energy distribution in the structure. For the sake of simplicity we neglect the frequency dependence of the model parameters in this paragraph.

The actual performance of a MACOR absorber at TTF-2 will be discussed in paragraph IIIb). In this paragraph we take the proper frequency dependence of all parameters into account. This includes the complex permittivity spectra of MACOR which we measured most recently at the Institut für Physikalische Chemie in Münster.

IIIa) Validation of the developed method

In order to check the validity of the proposed matrix method several structures are investigated the parameters of which are given in Table 1 at the end of this paragraph. Note that these parameters do not correspond to real structures; they are rather chosen such that a certain effect can clearly be observed.

The first structure simply consists of a cavity section which is embedded between two beampipes. Except for the fact that photons are only generated in the cavity all three sections have the same parameters. Fig. 16 shows the energy and the power density of this configuration

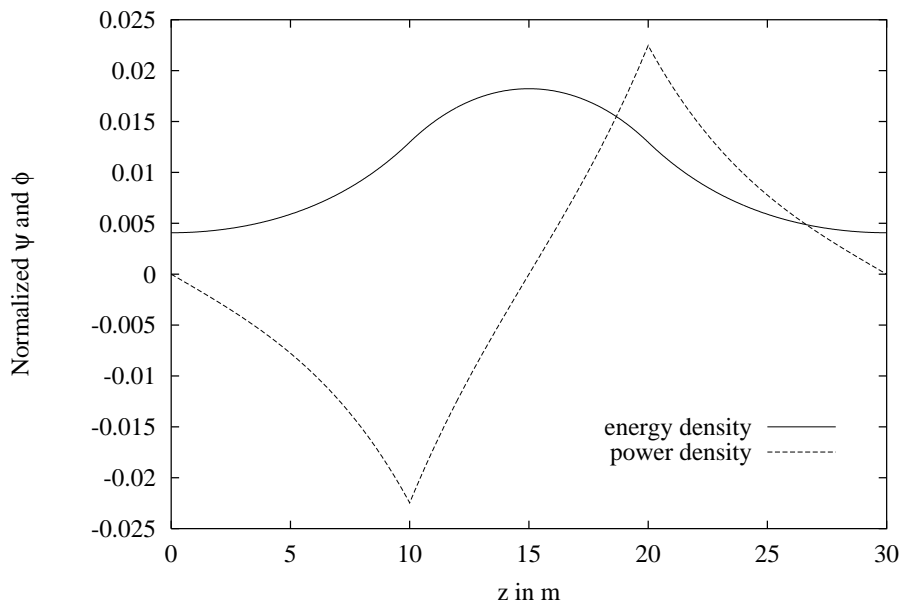


Figure 16: Energy and power density of the first structure as a function of the axial coordinate.

as a function of the axial coordinate z . The energy density is a smooth distribution with its maximum in the middle of the cavity. Furthermore the slope of this curve vanishes at the boundaries of the structure at $z = 0$ and $z = 30$ m. Due to its symmetry, the power density vanishes exactly at $z = 15$ m. Starting from this point, the absolute value of Φ increases until the ends of the cavity. Since it is assumed that the cavity section and the beampipes have the same diameter the power density is continuous at the beampipe-cavity transitions. However, the slope of this curve changes at the transitions because no photon generation takes place in the beampipes. At the beginning and at the end of the structure Φ vanishes as required by the boundary conditions according to Eq.(49).

In paragraph IIb.2) it was claimed that we may assume a diffusion constant for the beampipes which is much larger than that for a TESLA cavity leading to an approximately constant energy density in the beampipes. In order to check this statement let us consider the second structure which is basically identical to the first one except for the diffusion constants of the beampipe sections. For the first structure we used a uniform diffusion constant of $1 \cdot 10^3$ m²/s for all sections. On the other hand we assume for the second structure that the diffusion constant for the beampipes is $1 \cdot 10^5$ m²/s which is two orders of magnitude higher than that for the cavity. Fig. 17 presents the energy and the power distribution for this case. Both curves are

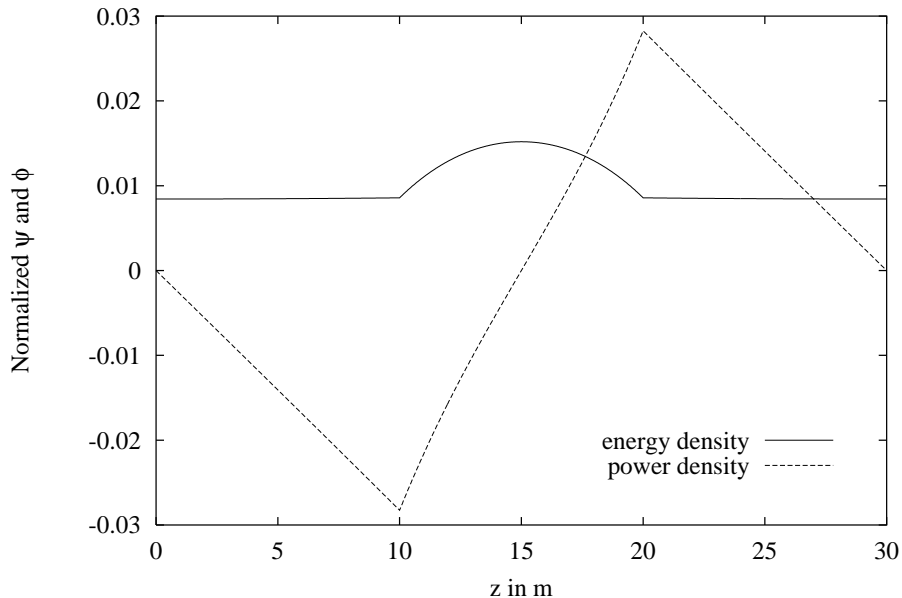


Figure 17: Energy and power density of the second structure as a function of the axial coordinate.

very similar to those of the previous structure inside the cavity. In the beampipes, however, the energy density stays indeed almost constant. The corresponding power density is approximately a linear function of the axial coordinate. If we further increase D in the beampipes, e.g. to $1 \cdot 10^7$ m²/s, we get nearly the same curves for Ψ and Φ which confirms our assertion from paragraph IIb.2) that the results of the diffusion model do not depend on the exact value of D for the beampipes.

In paragraph IIb.3) the diffusion model parameters of an absorber were discussed. There it was shown that a small damping time is a feature of an absorber. The damping time of a MACOR pipe is in the nanosecond-range whereas the cavity damping time is approximately

30 ms. In order to study the effect of a small τ let us reduce its value for the first and the third section to $10 \mu\text{s}$. Initially a uniform value of 30 ms was used for all sections. Fig. 18 shows the

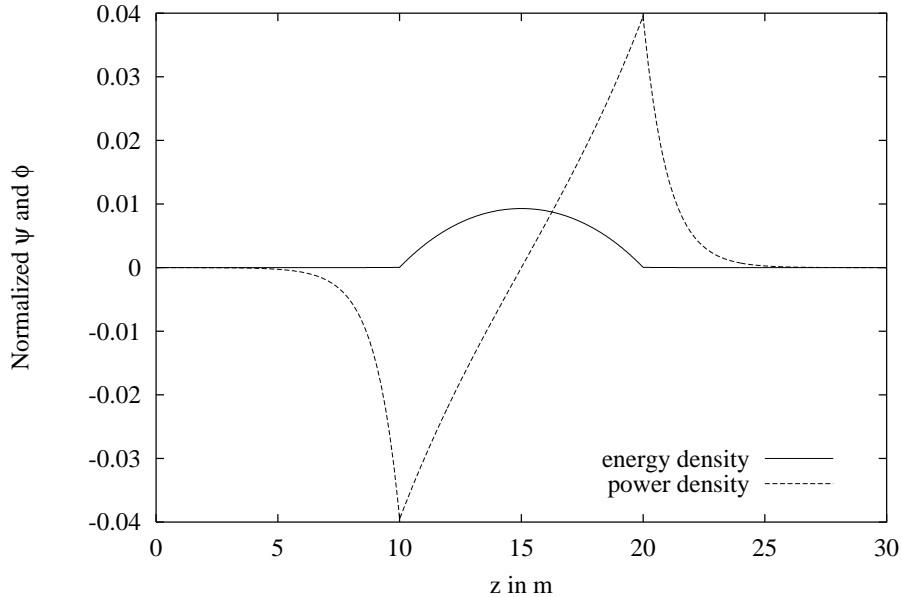


Figure 18: Energy and power density of the third structure as a function of the axial coordinate.

corresponding plot of Ψ and Φ as a function of z . The energy densities in the first and the third section decay rapidly due to the reduced damping time which correspond to a large loss of photons. Within a distance of 5 m from the cavity the energy density drops almost to zero. This already indicates that even a short absorber may work efficiently because the damping time of a MACOR pipe is much less than $10 \mu\text{s}$.

We still have to check if changes of the cross section of the structure are properly taken into account. Let us therefore assume that the radius of the beampipes is twice as large than that of the cavity section. For this discussion it is convenient to consider besides Ψ and Φ also the power, which is the integral of Φ over the cross section of the structure, as a function of z . Fig. 19 shows the corresponding curves for the fourth structure. The power distribution is continuous at the cavity-beampipe transitions at $z = 10 \text{ m}$ and $z = 20 \text{ m}$ as it should be. On the other hand the power density has step discontinuities at these points according to Eq. (46), namely $\Phi_{01}^2 = 4 \cdot \Phi_{02}^1$ and $\Phi_{01}^3 = 0.25 \cdot \Phi_{02}^2$ because $r^1 = r^3 = 2 \cdot r^2$.

In order to show how a HOM absorber works let us go back to the second structure. In this structure we install a 1 m long HOM absorber in the middle of the beampipe at the R.H.S. of the cavity. We assume that the absorber pipe has the same diffusion constant as the beampipe but a reduced damping time of $10 \mu\text{s}$. The radius of the absorber pipe is slightly larger than that of the beampipe in order to keep the short range wake of the HOM absorber small. The parameters of the entire configuration are also given in Table 1.

The energy density of the second structure and that of the corresponding one with absorber are compared in Fig. 20. This figure demonstrates that the absorber catches almost all photons and pulls Ψ down to zero at the location where it is placed. This leads also to a considerable reduction of the energy density in the cavity itself. Fig. 21 compares the power density of the second structure with that of the fifth one. Behind the absorber the power density is zero.

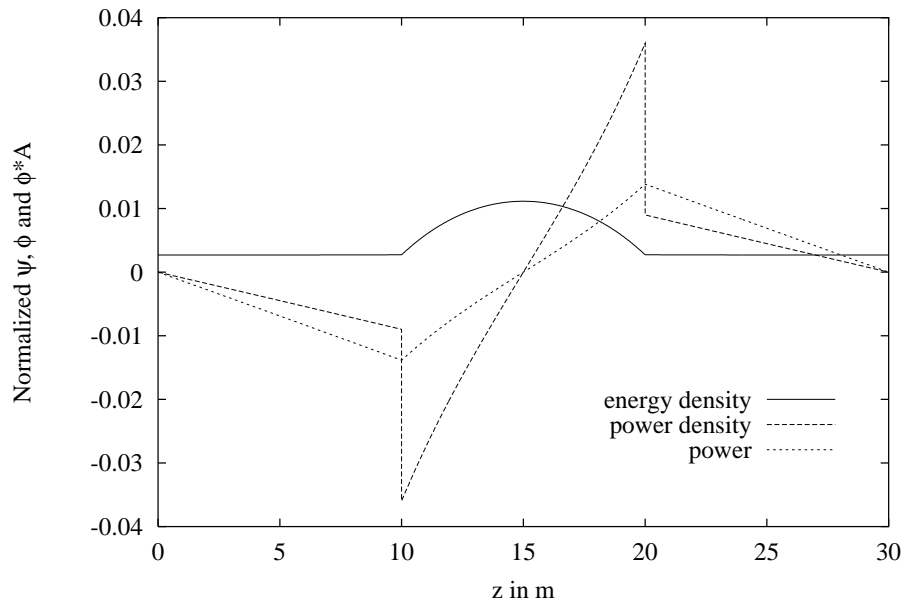


Figure 19: Energy density, power density and power of the fourth structure as a function of the axial coordinate.

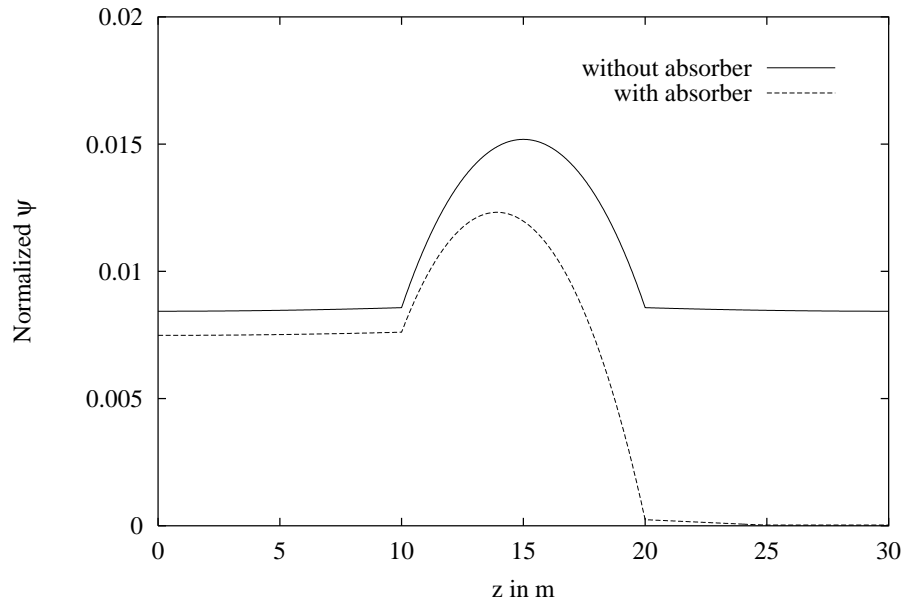


Figure 20: Comparison between the photon density of the second structure and that of the same structure with absorber.

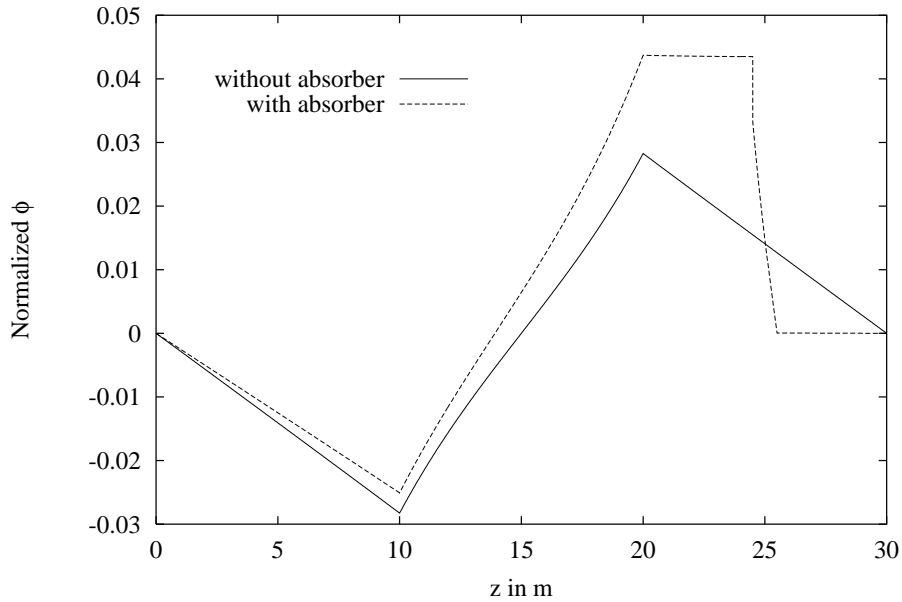


Figure 21: Comparison between the photon flux density of the second structure and that of the same structure with absorber.

On the other hand, in front of the absorber it is significantly higher than that of the second structure. This confirms the idea that the HOM absorber also attracts photons from the cavity.

IIIb) Absorber performance at TTF-2

It is planned to investigate the performance of a HOM absorber experimentally in TTF-2. The absorber is to be installed somewhere downstream from the last accelerating module M8, see Fig. 22. As a first test it is foreseen to use the absorber at room temperature which can easily be done. Since its performance strongly depends on its operational temperature, which has been discussed above, it also seems to be reasonable to check if it still works when it is cooled in a bath of liquid nitrogen. Thus we will give results for the absorber losses for both temperature levels.

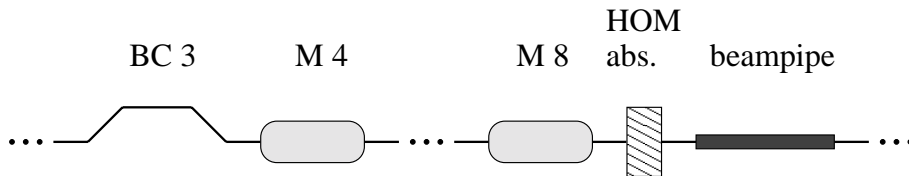


Figure 22: Schematics of that part of TTF-2 which is important for the performance of a HOM absorber.

For a high absorber efficiency it is obvious that we have to keep the distance between the cavities, where the photons are generated, and the absorber as small as possible. The minimum gap between the cavities of M8 and the absorber seems to be roughly 2.5 m. For this section we assume a steel beampipe at room temperature.

First structure					
sec. #	r^n in mm	L^n in m	D^n in m^2/s	τ^n in s	phot. gen.
1	35	10	$1 \cdot 10^3$	$30 \cdot 10^{-3}$	no
2	35	10	$1 \cdot 10^3$	$30 \cdot 10^{-3}$	yes
3	35	10	$1 \cdot 10^3$	$30 \cdot 10^{-3}$	no

Second structure					
sec. #	r^n in mm	L^n in m	D^n in m^2/s	τ^n in s	phot. gen.
1	35	10	$1 \cdot 10^5$	$30 \cdot 10^{-3}$	no
2	35	10	$1 \cdot 10^3$	$30 \cdot 10^{-3}$	yes
3	35	10	$1 \cdot 10^5$	$30 \cdot 10^{-3}$	no

Third structure					
sec. #	r^n in mm	L^n in m	D^n in m^2/s	τ^n in s	phot. gen.
1	35	10	$1 \cdot 10^5$	$10 \cdot 10^{-6}$	no
2	35	10	$1 \cdot 10^3$	$30 \cdot 10^{-3}$	yes
3	35	10	$1 \cdot 10^5$	$10 \cdot 10^{-6}$	no

Fourth structure					
sec. #	r^n in mm	L^n in m	D^n in m^2/s	τ^n in s	phot. gen.
1	70	10	$1 \cdot 10^5$	$30 \cdot 10^{-3}$	no
2	35	10	$1 \cdot 10^3$	$30 \cdot 10^{-3}$	yes
3	70	10	$1 \cdot 10^5$	$30 \cdot 10^{-3}$	no

Fifth structure					
sec. #	r^n in mm	L^n in m	D^n in m^2/s	τ^n in s	phot. gen.
1	35	10	$1 \cdot 10^5$	$30 \cdot 10^{-3}$	no
2	35	10	$1 \cdot 10^3$	$30 \cdot 10^{-3}$	yes
3	35	4.5	$1 \cdot 10^5$	$30 \cdot 10^{-3}$	no
4	40	1	$1 \cdot 10^5$	$10 \cdot 10^{-6}$	no
5	35	4.5	$1 \cdot 10^5$	$30 \cdot 10^{-3}$	no

Table 1: Parameters of the structures that were investigated in IIIa).

Bunch compressor 3 (BC3) is located in front of the string of the 5 accelerating cavities M4 . . . M8. It has a length of 24 m; and its vacuum chamber is normal conducting. This means that wakefields which are generated upstream BC3 are already absorbed within the bunch compressor. It is thus convenient to terminate our model with a sufficiently long beampipe section (20 m) at its L.H.S. Such a beampipe can also be used as a termination beyond the absorber because in TTF-2 everything downstream this device is normal conducting.

Between the modules we assume beampipe sections made out of steel and copper at a temperature of 4 K with a length of 0.5 m and 0.9 m, respectively. The steel sections represent the interconnections between the modules as well as the input couplers, the low frequency HOM couplers, the cavity beam position monitors and the two shutters which are foreseen for each module; and the copper sections correspond to the 0.9 m long copper-plated steel beampipe within the superconducting quadrupoles. For the cavity sections we assume a mean radius of 70 mm. Table 2 summarizes the parameters which we use for our model of TTF-2.

sec. #	r^n in mm	L^n in m	type	material	temp. in K
1	35	20	beampipe	steel	295
2	70	12	cavity	niobium	2
3	35	0.9	beampipe	copper	4
4	35	0.5	beampipe	steel	4
5	70	12	cavity	niobium	2
6	35	0.9	beampipe	copper	4
7	35	0.5	beampipe	steel	4
8	70	12	cavity	niobium	2
9	35	0.9	beampipe	copper	4
10	35	0.5	beampipe	steel	4
11	70	12	cavity	niobium	2
12	35	0.9	beampipe	copper	4
13	35	0.5	beampipe	steel	4
14	70	12	cavity	niobium	2
15	35	0.9	beampipe	copper	4
16	35	2.5	beampipe	steel	295
17	40	0.1	absorber	MACOR	88 or 295
18	35	20	beampipe	steel	295

Table 2: Parameters of our model for TTF-2.

Applying the matrix formulation, we calculated the HOM losses in the MACOR absorber. Fig. 23 shows the absorbed power at room temperature as a function of the bunch length with the thickness of the ring as a parameter. For the simulations 11315 bunches per bunch train with a bunch charge of 1 nC and a repetition frequency of 5 Hz are assumed. The presented HOM losses belong to a frequency range from 20 GHz to 1 THz. Above the upper frequency

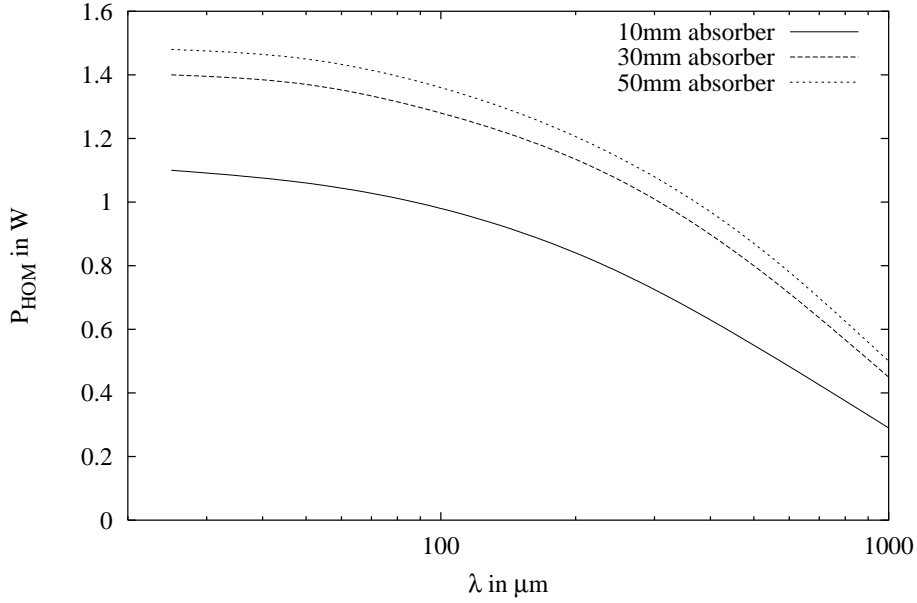


Figure 23: Power absorption of a MACOR absorber at room temperature in TTF-2 as a function of the bunch length with the thickness of the absorber ring as a parameter.

limit no significant HOM losses are observed. On the other hand, the beam excites a non-negligible amount of wakefields below 20 GHz; roughly 50% of the HOM losses correspond to this frequency range. Unfortunately these losses cannot be treated using the photon diffusion model because it applies only to sufficiently high frequencies.

The power absorbed by the MACOR ring drops continuously with increasing bunch length. It gets however quite independent from λ for bunches shorter than $100 \mu\text{m}$. The three curves which are presented in Fig. 23 show that the absorber efficiency can considerably be improved, especially for long bunches, if we use a MACOR ring with a thickness of 30 mm instead of a 10 mm thick one. On the other hand a further increase of the outer diameter of the ring leads only to a slight increase of the absorbed power. In Fig. 24 corresponding results for a MACOR absorber at 88 K are presented. The basic difference to the previous case is that the power absorption at the low temperature level is significantly less than that at room temperature.

During operation of TTF-2 we intend to measure the temperature rise of the absorber ring in order to estimate the absorbed power. Fig. 25 schematically shows the installation of the ring absorber. Let us assume that its L.H.S. is mounted to a housing with a fixed temperature T_b . Then the HOM losses heat up the MACOR ring. If the losses are uniformly distributed along the axial coordinate the temperature distribution in the absorber can approximately be written as

$$T(z) - T_b = P_{HOM} R \left(\frac{z}{L} - \frac{z^2}{2L^2} \right) \quad , \quad (65)$$

where R and P_{HOM} denote the thermal resistance of the MACOR cylinder and the HOM losses. The heat resistance of such a cylinder is given by

$$R = \frac{L}{\lambda \pi (r_o^2 - r_i^2)} \quad , \quad (66)$$

where r_o , r_i and λ are the outer and the inner radius of the cylinder and the thermal conductivity

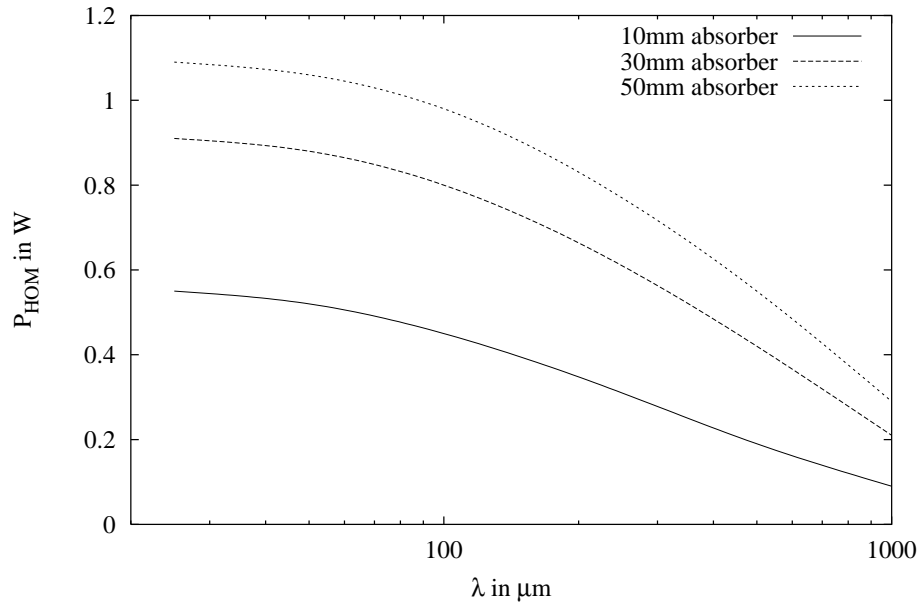


Figure 24: Power absorption of a MACOR absorber at 88 K in TTF-2 as a function of the bunch length with the thickness of the absorber ring as a parameter.

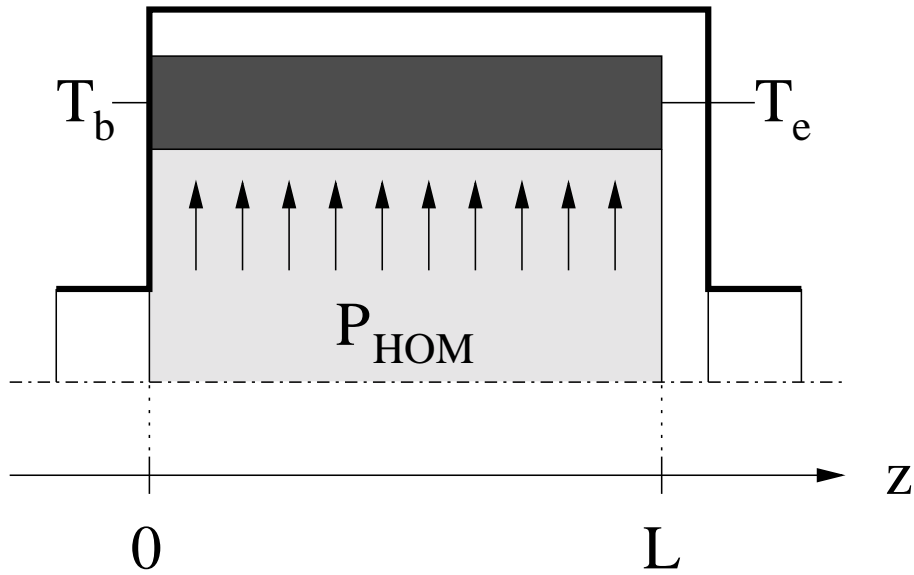


Figure 25: Schematics of the installation of a MACOR ring absorber.

of the absorber material, respectively. For MACOR at room temperature λ is $1.5 \text{ W} / (\text{K m})$. Fig.26 presents the temperature distribution in the absorber for a typical example. We will

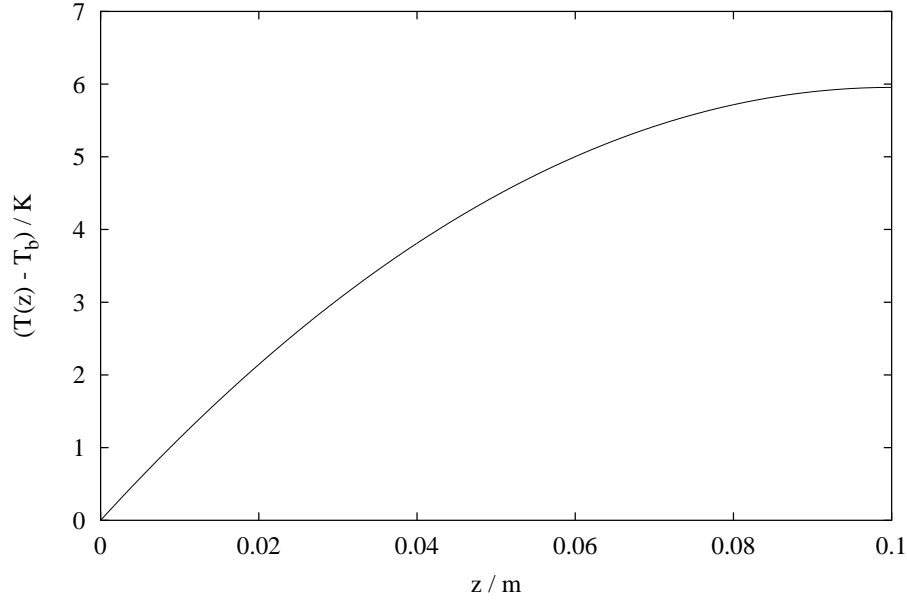


Figure 26: Temperature distribution in a ring absorber. Parameters: $L = 0.1 \text{ m}$, $r_i = 44 \text{ mm}$, $r_o = 54 \text{ mm}$, $\lambda = 1.5 \text{ W}/(\text{K m})$, $P_{HOM} = 0.55 \text{ W}$.

install a temperatur sensor close to the end of the absorber where the largest temperature difference $\Delta T = T_e - T_b$ is observed. It can be calculated from Eq.(65) by setting $z = L$:

$$\Delta T = \frac{1}{2} P_{HOM} R \quad (67)$$

In order to calculate ΔT for the cases which were already discussed in Figs.23 and 24 we have to take into account the thermal resistance of the different MACOR cylinders. In Table 3 this quantity is given for the absorber rings of Figs. 23 and 24 assuming the heat conductivity of

Thickness of the MACOR ring in mm	10	30	50
Thermal resistance in K / W	10.83	3.00	1.54

Table 3: Thermal resistance of various MACOR rings. Parameters: $L = 0.1 \text{ m}$ and $r_i = 44 \text{ mm}$.

MACOR at room temperature. Since we have no data of R for MACOR at other temperatures we also use the value of $1.5 \text{ W} / (\text{K m})$ at 88 K .

Figs.27 and 28 show ΔT as a function of the bunch length for the 10 mm, the 30 mm and the 50 mm absorber ring at 295 K and 88 K . Note that the largest temperature differences are obtained using the thinnest absorber ring because the thermal resistance of such a ring is higher than that of the thicker rings. Depending on the bunch length and the temperature level of the absorber material, ΔT lies roughly between 1 K and 10 K for the 10 mm ring. Such a temperature rise can easily be measured with standard thermal sensors.

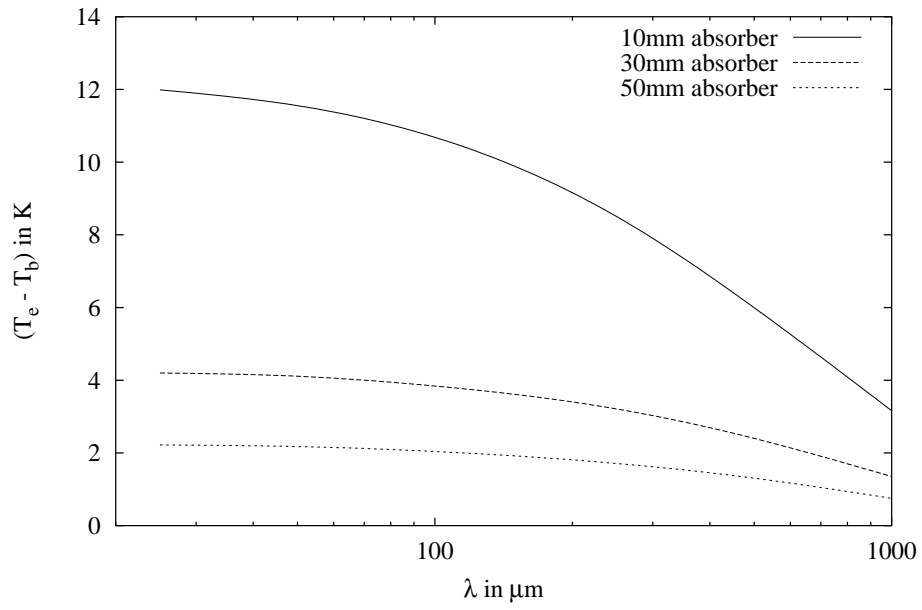


Figure 27: Temperature difference over a MACOR absorber at room temperature in TTF-2 as a function of the bunch length with the thickness of the absorber ring as a parameter.

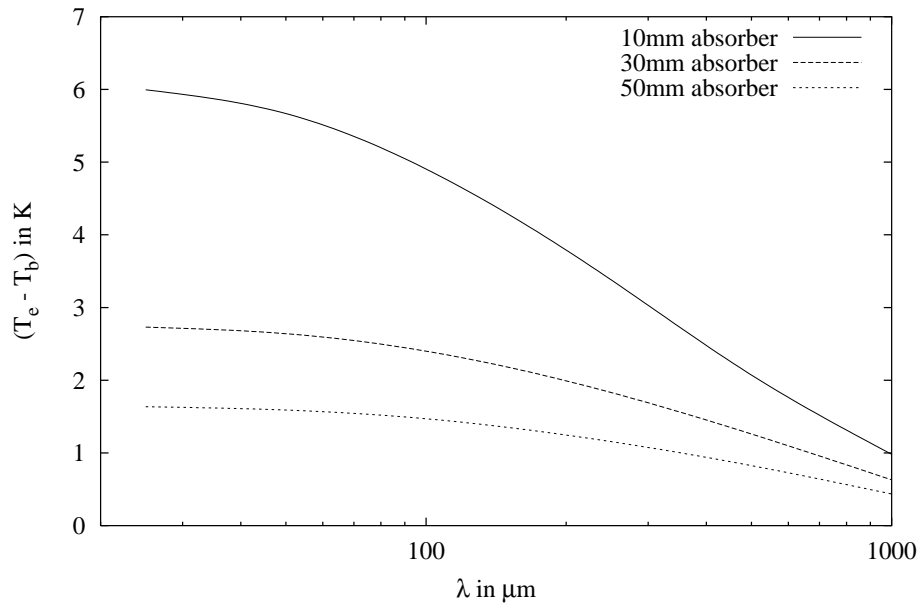


Figure 28: Temperature difference over a MACOR absorber at 88 K in TTF-2 as a function of the bunch length with the thickness of the absorber ring as a parameter.

IV Conclusions

A diffusion model has been presented which may be used to calculate the steady state photon density in an accelerating structure consisting of beam pipe, cavity and absorber sections for high frequencies. The validity of the model has been extensively checked. Then it has been applied to investigate the performance of a HOM MACOR absorber in TTF-2. The simulations require the complex permittivity of the absorber material in the frequency range from some GHz up to the THz regime. The permittivity of MACOR has been measured from 300 GHz to approximately 1.5 THz at 88 K and 295 K using a FTIR-spectrometer. Combining the measurement results with numbers from the literature, it has been found that the temperature rise of the proposed MACOR absorber at room temperature due to HOM losses is in the order of some degrees. So it should easily be possible to measure the effect of the absorber using a standard temperature sensor. Corresponding simulations with MACOR at 88 K have predicted an increase of the absorber temperature which still amounts to about half of that of the 295 K case. This result is however based on an extrapolation of the MACOR losses to low frequencies because the electrical properties of this material have not yet been measured in this spectral range for an absorber temperature of about 70 K.

Acknowledgement

The authors are indebted to many colleagues from the TESLA collaboration who contributed to these ideas.

References

- [1] A. Jöstingmeier, M. Dohlus, M. Wendt and C. Cramer, “Theoretical and practical investigations concerning the design of a HOM broadband absorber for TESLA”, DESY, TESLA 2000-10, 2000.
- [2] A. Novokhatski, M. Timm and T. Weiland, “Single bunch energy spread in the TESLA cryomodule”, DESY, TESLA 99-16, 1999.
- [3] R. E. Collin, *Foundations for Microwave Engineering*, McGraw-Hill, 1966.
- [4] R. Brinkmann, M. Dohlus, D. Trines, A. Novokhatski, M. Timm, T. Weiland, P. Hülsmann, C. T. Rieck, K. Scharnberg and P. Schmüser, “Terahertz wakefields in the superconducting cavities of the TESLA-FEL linac”, DESY, TESLA 2000-07, 2000.

Appendix

This paragraph is intended to give a broad description of how we measured the material properties of MACOR using a BOMEM FTIR-spectrometer DA8.1 which is equipped with various sources, beam splitters and detectors. In the frequency range under investigation (300 GHz to roughly 1.5 THz) we used a mercury lamp (source), a 125 μm Mylar film (beam splitter) and a bolometer (detector). All spectra taken were transmission spectra of samples of different thickness (200 μm to 2.8 mm).

The central part of the FTIR-spectrometer is a Michelson Fourier interferometer which is illustrated in Fig. 29. The interferometer is illuminated with the broad band source spectrum of

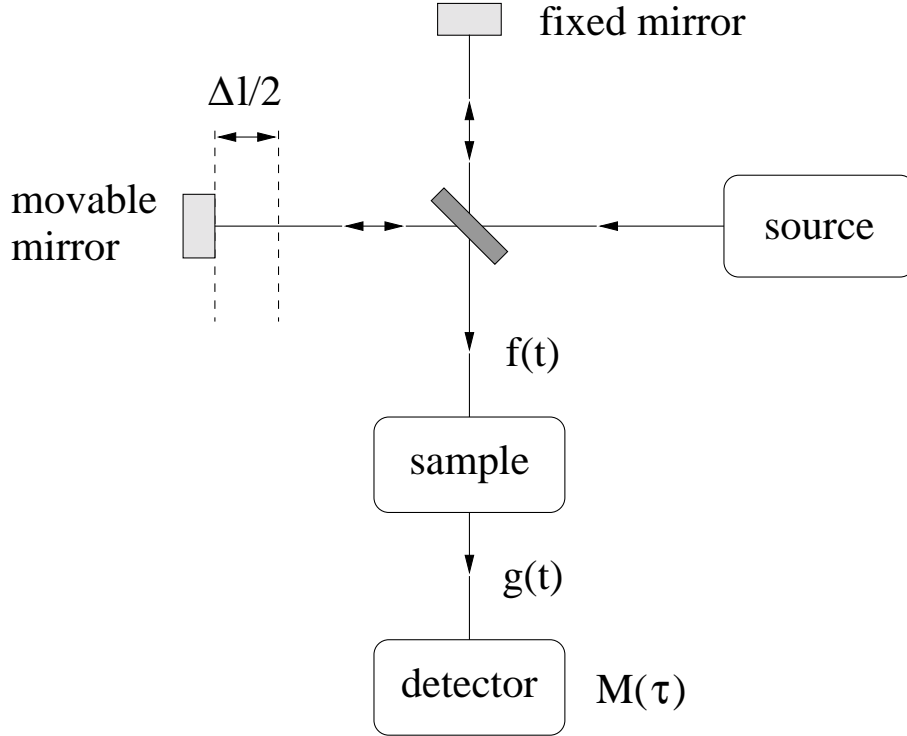


Figure 29: Schematics of the FTIR-spectrometer.

the Hg-lamp. A special feature of a Fourier interferometer is that one of its mirrors is continuously moved. Shifting the moveable mirror by $\Delta l/2$ retards the signal in this arm by $\tau = \Delta l/c_0$. Let $s(t)$ denote the signal in the output arm due to the reflection at the fixed mirror which is proportional the source signal. Superimposing the reflections from both mirrors yields

$$f(t) = s(t - \tau) + s(t) \quad . \quad (68)$$

Eq. (68) means that if the interferometer was fed by a monochromatic source with a frequency f we would have $f(t) = 2s(t)$ for $\tau = n/f$ and $f(t) = 0$ for $\tau = (n + \frac{1}{2})/f$, where n denotes a natural number. The signal $f(t)$ passes then a planar sample of the test material. This process may be described in time domain by a convolution of $f(t)$ with the delta-response $h(t)$ which corresponds to the transmission of an electromagnetic pulse through a dielectric layer:

$$g(t) = f(t) \otimes h(t) \quad (69)$$

Let us finally assume that the detector output M equals the energy which is contained in $g(t)$:

$$M(\tau) = \int_{t=-\infty}^{\infty} g^2(t) dt \quad (70)$$

Note that the detector signal is still a function of τ which is essential for the understanding of working principle of a Fourier interferometer.

The question which arises now is how do we get the desired material properties of the sample from the measured $M(\tau)$. Let us split the answer into two steps:

- Determination of the transfer function $H(j\omega) = \mathcal{F}\{h(t)\}$.
- Calculation of the material properties from $H(j\omega)$.

If we write Eq. (70) in frequency domain we get

$$M(\tau) = \frac{1}{2\pi} \int_{\omega=-\infty}^{\infty} |G(j\omega)|^2 d\omega \quad , \quad (71)$$

where $g(t)$ and $G(j\omega)$ are related by $G(j\omega) = \mathcal{F}\{g(t)\}$. The convolution of Eq. (69) is equivalent to a multiplication of the corresponding spectra in frequency domain. Let furthermore $S(j\omega)$ be the spectrum of $s(t)$. Then we can rewrite Eq. (71) as

$$M(\tau) = \frac{1}{2\pi} \int_{\omega=-\infty}^{\infty} |H(j\omega)|^2 |S(j\omega) + S(j\omega) e^{-j\omega\tau}|^2 d\omega \quad , \quad (72)$$

where the delay of τ in the arm with the moveable mirror is taken into account by the factor $e^{-j\omega\tau}$. Reorganizing the above equation yields

$$M(\tau) = \frac{1}{2\pi} \int_{\omega=-\infty}^{\infty} |H(j\omega)|^2 |S(j\omega)|^2 (2 + 2\cos(\omega\tau)) d\omega \quad . \quad (73)$$

If we apply a Fourier transformation to both sides of Eq. (73) we arrive at

$$|H(j\omega)|^2 |S(j\omega)|^2 = \int_{\tau=0}^{\infty} M(\tau) \cos(\omega\tau) d\tau \quad \text{for } \omega \neq 0 \quad . \quad (74)$$

This means that the spectrum $|H(j\omega)| |S(j\omega)|$ (except for its dc-component) is given by a Fourier transformation of the detector signal with respect to the delay time τ . The still unknown function $|S(j\omega)|$, which depends on the spectrum delivered by the signal source and on the frequency characteristics of the optical elements of the interferometer, can be eliminated by one calibration measurement without absorber material. In a real device the mirror can of course not be moved from zero to infinity. The interferometer works within a finite range for τ which limits the frequency resolution of the measurements.

For the further discussion let us assume that $|H(j\omega)|$ is known for two samples with different thickness. Unfortunately one cannot calculate $\varepsilon'_r(\omega)$ and $\varepsilon''_r(\omega)$ of the test material analytically from the measured transfer functions. Thus a simulation routine is used which allows to “optimize” $\varepsilon'_r(\omega)$ and $\varepsilon''_r(\omega)$ such that the computed functions $|H(j\omega)|$ match the measured ones. The measurement of two samples is required in order to get a unique result.